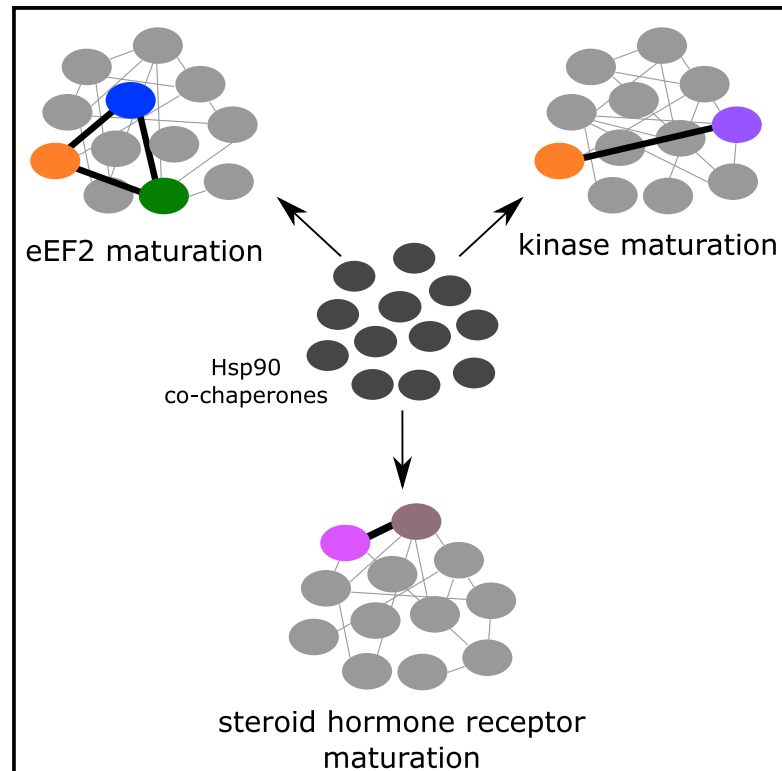


Hsp90 Co-chaperones Form Plastic Genetic Networks Adapted to Client Maturation

Graphical Abstract



Authors

Maximilian M. Biebl, Maximilian Riedl, Johannes Buchner

Correspondence

johannes.buchner@tum.de

In Brief

Biebl et al. show that Hsp90 co-chaperones form client-specific genetic networks for client maturation. Tightly interacting core genetic modules of co-chaperones specific for a client are embedded in a network of looser genetic interactions. Distinct epistatic Hsp90 co-chaperone modules regulate kinase activation, steroid hormone receptor maturation, and protein biosynthesis.

Highlights

- Genetic interactions between Hsp90 co-chaperones are dynamic and client specific
- Sti1, Cpr7, and Cns1 form an epistatic module maintaining eEF2 integrity
- Sti1/Hsp70 and Cdc37 act on two parallel pathways for kinase maturation
- Aha1 and Hch1 are dwell-time regulators for Hsp90 client complexes



Article

Hsp90 Co-chaperones Form Plastic Genetic Networks Adapted to Client Maturation

Maximilian M. Biebl,¹ Maximilian Riedl,¹ and Johannes Buchner^{1,2,*}¹Center for Integrated Protein Science at the Department of Chemistry, Technische Universität München, Lichtenbergstrasse 4, 85747 Garching, Germany²Lead Contact*Correspondence: johannes.buchner@tum.de<https://doi.org/10.1016/j.celrep.2020.108063>**SUMMARY**

Heat shock protein 90 (Hsp90) is a molecular chaperone regulating the activity of diverse client proteins together with a plethora of different co-chaperones. Whether these functionally cooperate has remained enigmatic. We analyze all double mutants of 11 *Saccharomyces cerevisiae* Hsp90 co-chaperones *in vivo* concerning effects on cell physiology and the activation of specific client proteins. We find that client activation is supported by a genetic network with weak epistasis between most co-chaperones and a few modules with strong genetic interactions. These include an epistatic module regulating protein translation and dedicated epistatic networks for specific clients. For kinases, the bridging of Hsp70 and Hsp90 by Sti1/Hop is essential for activation, whereas for steroid hormone receptors, an epistatic module regulating their dwell time on Hsp90 is crucial, highlighting the specific needs of different clients. Thus, the Hsp90 system is characterized by plastic co-chaperone networks fine-tuning the conformational processing in a client-specific manner.

INTRODUCTION

Heat shock protein 90 (Hsp90) is an abundant and conserved molecular chaperone present in bacteria and eukaryotes (Johnson, 2012). Together with a large number of co-chaperones, it plays a pivotal role in the maturation of client proteins under physiological and stress conditions (Schopf et al., 2017). Clients include steroid hormone receptors (SHRs), kinases, and E3 ubiquitin ligases, which rely on Hsp90 interaction for activity (Boczek et al., 2015; Echeverría et al., 2011; McClellan et al., 2007; Taipale et al., 2012). In contrast to other chaperones, Hsp90 acts late in the maturation process and also seems to have a regulatory role (Jakob et al., 1995; Nathan and Lindquist, 1995; Nathan et al., 1997; Radli and Rudiger, 2018). Because Hsp90 controls central hubs of cellular protein homeostasis, it has an important role in diseases such as cancer, neurodegenerative disease, and psychiatric disorders (Biebl and Buchner, 2019; Joshi et al., 2018).

Hsp90 is a constitutive dimer with a V-shaped structure (Ali et al., 2006; Pearl and Prodromou, 2006; Shiau et al., 2006), which undergoes an ATP-driven conformational cycle that comprises large structural rearrangements, including a transiently N-terminally dimerized conformation (Prodromou et al., 2000; Verba et al., 2016). In eukaryotes, the conformational cycle is modulated by the binding of co-chaperones that vary in structure, function, and specificity for certain Hsp90 conformations (Li et al., 2012). While the co-chaperome expanded from yeast to mammals, similar functions have been found for the orthologs, suggesting that new co-chaperones added regulatory mechanisms (Johnson and Brown, 2009). In yeast, many co-chaperones modulate the chaperone function of Hsp90 (Table 1). Only three of them are

essential (Cdc37, Cns1, and Sgt1). For some co-chaperones, their function in the Hsp90 cycle is well described. Sti1/Hop acts early in the Hsp90 chaperone cycle connecting the Hsp70 and Hsp90 systems and keeping Hsp90 in an open, client-accessible state (Chen and Smith, 1998; Johnson et al., 1998; Kirschke et al., 2014; Schmid et al., 2012). Notably, direct contacts between Hsp70 and Hsp90 have been reported in bacteria and yeast (Genest et al., 2013; Kravats et al., 2018). For kinases, Cdc37 is a specific recruiter co-chaperone (Abbas-Terki et al., 2000; Eckl et al., 2013; Grammatikakis et al., 1999; Taipale et al., 2012; Verba et al., 2016). Other co-chaperones, like Sba1/p23, act late in the Hsp90 cycle and stabilize the N-terminally dimerized state (Ali et al., 2006; McLaughlin et al., 2006; Richter et al., 2004). Notably, for some co-chaperones, like p23, Hsp90-independent functions have been observed (Bose et al., 1996; Echtenkamp et al., 2016; Freeman et al., 1996).

Previously, we found that the maturation of different Hsp90 clients depends on different co-chaperones in yeast (Sahasrabudhe et al., 2017). Surprisingly, for a specific client, co-chaperones may have either activating or deactivating effects - or they may have no effect at all. This led to the picture of a machinery in which the different parts are individually recruited in a client-specific way. Yet, we do not know how the co-chaperones are coordinated and to what extent they cooperate in client processing. Large-scale screening projects (Costanzo et al., 2016; Rizzolo et al., 2017, 2018) do not provide information on this issue, as these fitness-based screens cannot predict functional relationships between genes. To address the question whether each co-chaperone contributes independently to client maturation or whether the contribution of one co-chaperone affects other



Table 1. Hsp90 Co-chaperones in Yeast

Yeast Co-chaperone	Human Homolog	Function	References
Sti1	Hop	adaptor between Hsp70 and Hsp90; inhibitor of Hsp90 ATPase	Kirschke et al., 2014; Lee et al., 2012; Röhl et al., 2015; Schmid et al., 2012
Cdc37	Cdc37	kinase-specific co-chaperone	Boczek et al., 2015; Siligardi et al., 2002
Cns1	TTC4	genetic interaction with Cpr7; regulator of protein translation	Schopf et al., 2019; Tenge et al., 2015
Tah1	Tah1	component of the Rvb1-Rvb2-Tah1-Pih1 (R2TP) complex	Eckert et al., 2010
Pih1	Pih1		
Cpr6	Cyp40	peptidylprolyl-cis/trans-isomerase	Mayr et al., 2000
Cpr7			
Sba1	p23	binds closed Hsp90 conformation, inhibits ATPase	Ali et al., 2006; McLaughlin et al., 2006; Richter et al., 2004
Aha1	Aha1	accelerator of Hsp90 ATPase	Meyer et al., 2004; Panaretou et al., 2002
Hch1	–	weak accelerator of Hsp90 ATPase	Panaretou et al., 2002
Ppt1	PP5	phosphatase interacting with Hsp90	Wandinger et al., 2006
Sgt1	Sgt1	involved in kinetochore assembly and plant immunity	Johnson et al., 2014; Kitagawa et al., 1999

co-chaperones is important to understand the functional principles of the Hsp90 chaperone machinery. Hence, we set out to systematically investigate genetic interactions between Hsp90 co-chaperones in *S. cerevisiae* on the functional level, i.e., in the activation of specific client proteins *in vivo*.

We used yeast as a model organism to analyze the function of co-chaperones on the maturation of the clients v-Src, glucocorticoid receptor (GR), and mineralocorticoid receptor (MR). The yeast Hsp90 system faithfully recapitulates the function of the mammalian co-chaperones on their clients (Bohen and Yamamoto, 1993; Chang and Lindquist, 1994; Fang et al., 1996; Picard et al., 1990; Xu and Lindquist, 1993), and most Hsp90 co-chaperones are conserved in structure and function between yeast and mammals (Koulov et al., 2010; McLaughlin et al., 2006; Meyer et al., 2003; Panaretou et al., 2002; Retzlaff et al., 2010; Röhl et al., 2015). Further, the system lacks biological processes that could influence reporter activity, such as downstream effectors of client activity. Since the aim of this study is to investigate the interplay between Hsp90 co-chaperones, it is beneficial that additional processes that affect SHR activity are missing in yeast. In addition, yeast abolishes inconsistencies due to the heterogeneity observed between and even within mammalian cell lines (Ben-David et al., 2018; Frattini et al., 2015; Liu et al., 2019; Rodina et al., 2016). Testing all possible knockouts (KOs) or knockdowns (KDs) of two co-chaperones concerning client maturation, we found that co-chaperone networks exist. In this framework, a few co-chaperones form strong genetic interactions, while the majority of co-chaperones cooperate loosely and add a client-specific layer of regulation. We identified epistatic modules that regulate protein biosynthesis, SHR maturation, and kinase activity.

RESULTS

Strain Generation and Validation

The yeast Hsp90 machinery comprises a cohort of well-characterized co-chaperones (Cox and Johnson, 2018; Li et al., 2011;

Sahasrabudhe et al., 2017; Siligardi et al., 2004; Smith and Toft, 1993). However, a comprehensive understanding of their genetic and functional interaction is still missing. To close this gap, we generated double KOs or KDs of 11 known co-chaperones in *S. cerevisiae* (Table 1). For the essential Cdc37 and Cns1 co-chaperones, DAMP (decreased abundance by mRNA perturbation) strains were used, in which protein levels are decreased by mRNA destabilization (i.e., *cdc37** and *cns1**) (Schuldiner et al., 2005). We mated the respective single-mutant strains with each other, and haploid double mutants were selected, resulting in 110 double mutants, comprising inherent biological duplicates of each double-mutant strain due to KO/KD of the same gene with different resistance cassettes (e.g., *sti1Δ::NatMX*, *sba1Δ::KanMX4* and *sti1Δ::KanMX4*, and *sba1Δ::NatMX*). All double mutants were viable during selection, suggesting that potential negative genetic interactions within the Hsp90 co-chaperone system do not lead to severe growth phenotypes.

To validate the generated double mutants, we first screened for growth defects. We performed spot assays with serial dilutions, quantified spot density, and normalized viability to the wild-type (WT) strain on the same plate. At 30°C, we detected growth defects for the *pih1Δ* and *cpr7Δ* single mutants, confirming previous studies (Deutschbauer et al., 2005; Duina et al., 1996b). To quantitate the effects of the double mutants on cell growth and obtain insight in the genetic interactions between co-chaperones, we calculated ϵ -scores (Elena and Lenski, 1997; Mani et al., 2008). This factor represents the difference between the survival/growth expected for the individual single mutants and the observed growth of the double mutant (Figure S1A). An ϵ -score of 0 indicates that there is no genetic interaction. A positive value points to a buffering interaction (the combined phenotype is less severe than expected) and is indicative of genes involved in the same pathway or protein complex. Negative scores reveal an aggravating effect (synthetic sick/lethal, negative genetic interaction; the combined phenotype is more severe than expected) and may hint toward parallel, compensatory pathways (Collins et al., 2007; Mani et al., 2008). Concerning

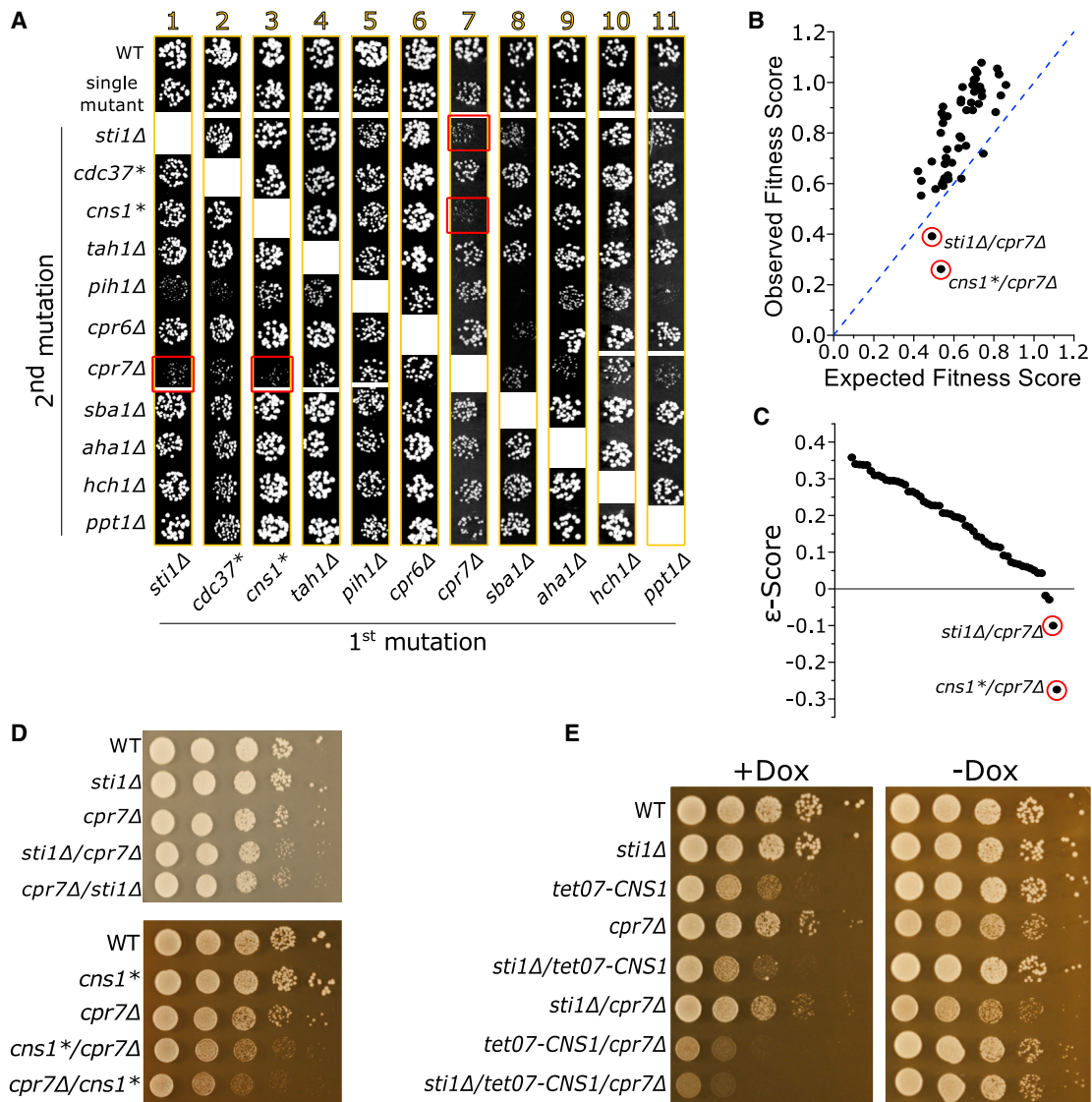


Figure 1. Hsp90 Co-chaperones Form a Robust Genetic Network

(A) Screen for genetic interactions affecting viability. The viability of single and double mutants of Hsp90 co-chaperones was screened at 30°C by spotting serial 10-fold dilutions on YPD medium. Only one representative dilution is shown. All agar plates contained the WT and the single-mutant strain as control. Note that each column (1–11) in the figure originates from a single plate, allowing for growth comparison between the rows within a column. Synthetic sick mutants are highlighted in red boxes. All mutants were screened twice or thrice with comparable results.

(B) Correlation of observed and expected fitness. The viability was scored by quantification of spot density of a suitable dilution and the spot density was normalized to the density of the WT strain spotted on the same plate. Averages of the inherent replicates (e.g., *sti1Δ/cdc37** and *cdc37*/sti1Δ*) were calculated. The observed fitness score was plotted against the expected fitness score derived from multiplying the single-mutant fitness scores.

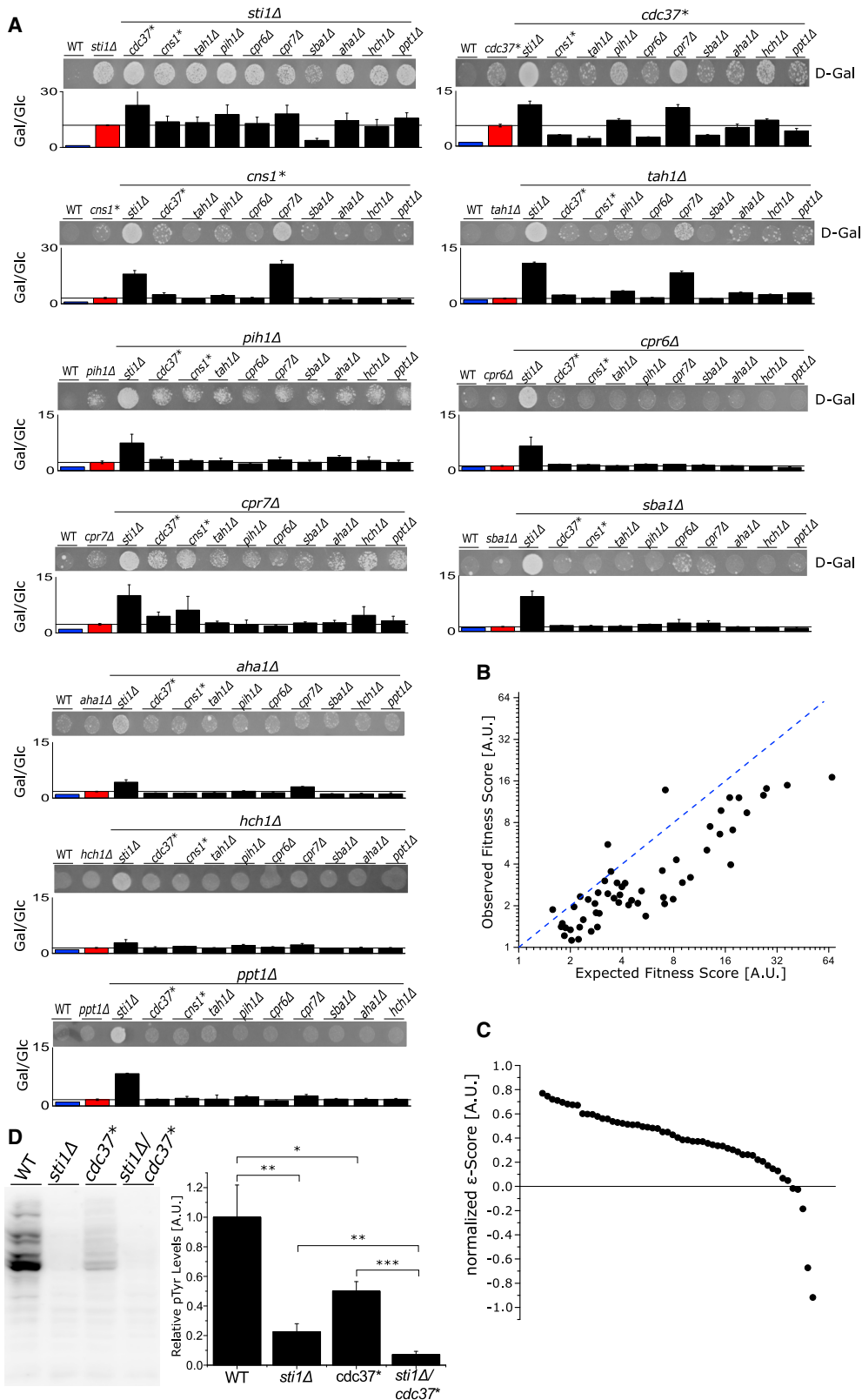
(C) ε-Score representation of double-mutant fitness. The spot quantifications of (B) were used to calculate the ε-score, defined as $\epsilon = f_{ab} - f_a \times f_b$, where f_{ab} indicates the fitness of the double mutant and f_a and f_b represent the fitness of the individual mutants. The synthetic sick mutants are labeled.

(D) Validation of negative genetic interactors. The negative genetic interactions of the *sti1Δ/cpr7Δ* and the *cns1*/cpr7Δ* strains were validated by drop dilution spot assays in 10-fold serial dilutions. The results are representative of three biological replicates.

(E) Validation of a tripartite epistatic module among *Sti1*, *Cns1*, and *Cpr7*. Drop dilution spot assays of the indicated yeast strains on agar supplemented with 10 μg/mL doxycycline (+Dox) are shown. The results are representative of biological triplicates.

the general fitness of *S. cerevisiae*, the majority of the double mutants displayed either no genetic interaction or positive genetic interactions, indicating a less severe phenotype than expected from the single mutants. Only two mutants displayed a strong

synthetic sick phenotype: *sti1Δ/cpr7Δ* ($\epsilon = -0.101$) and *cns1*/cpr7Δ* ($\epsilon = -0.275$) (Figures 1A–1D). Hence, the reduced fitness of the *cpr7Δ* strain was further aggravated by the loss of *Sti1* and *Cns1*, suggesting that *Cpr7* functions in common pathways



(legend on next page)

together with Sti1 and Cns1 (Schopf et al., 2019; Tenge et al., 2015). To confirm that Sti1, Cpr7, and Cns1 form an epistatic module, we tested whether Cns1 and Sti1 are also connected via a negative genetic interaction. We used a tet-off system for a more stringent KD of Cns1 than with the DAmP system (Schopf et al., 2019). Depletion of Cns1 via the tet-off system markedly reduced viability confirming that the KD efficiency exceeds that of the DAmP system (Figure 1E). Importantly, introduction of *sti1Δ* into the *tet07-CNS1* strain further reduced viability, confirming a negative genetic interaction between Sti1 and Cns1. Furthermore, the KO of *STI1* in the *tet07-CNS1/cpr7Δ* genetic background resulted in a synthetic sick mutant with strongly reduced fitness (Figure 1E). Hence, Sti1, Cns1, and Cpr7 form an epistatic module in which the co-chaperones are connected via negative genetic interactions with each other, extending previously found epistatic relationships of Cns1 with Cpr7 or Cpr7 with Sti1 (Duina et al., 1996a; Schopf et al., 2019).

To evaluate whether the synthetic sick double mutants showed growth defects due to impeded protein homeostasis or due to specific effects, we tested whether these mutants could still induce a heat shock response (HSR) after thermal stress (Figures S2A and S2B). As a marker, we used Hsp26 whose expression is increased upon heat shock (Kurtz et al., 1986). Our analysis showed that all mutants upregulated Hsp26 after heat stress at 42°C, suggesting that they still possess a functional HSR. Furthermore, global protein aggregation was not affected by the mutations, whereas inhibition of Hsp90 with radicicol led to a reduction of global protein aggregation, as previously described (Nathan et al., 1997), and heat shock at 42°C increased protein aggregation (Figures S2C–S2F). Additionally, we used scanning electron microscopy (SEM) to check yeast morphology. These analyses showed that the mutants displayed the same morphology as the WT (Figure S3A). Together, our results demonstrate that apart from the two strong negative genetic interactions between co-chaperones identified, the Hsp90 co-chaperone network is remarkably robust against the loss of co-chaperones.

Genetic Interactions of Co-chaperones Affecting Client Activity

Having established that general effects of the double-deletion strains on viability are largely lacking, we asked how specific functions in the context of the maturation of stringent Hsp90 cli-

ents are affected in the mutant strains. As model clients, we used the Hsp90-dependent oncogenic kinase v-Src (Boczek et al., 2015; Xu and Lindquist, 1993) and the two closely related Hsp90-dependent SHRs GR and MR (Dittmar et al., 1996; Smith and Toft, 1993).

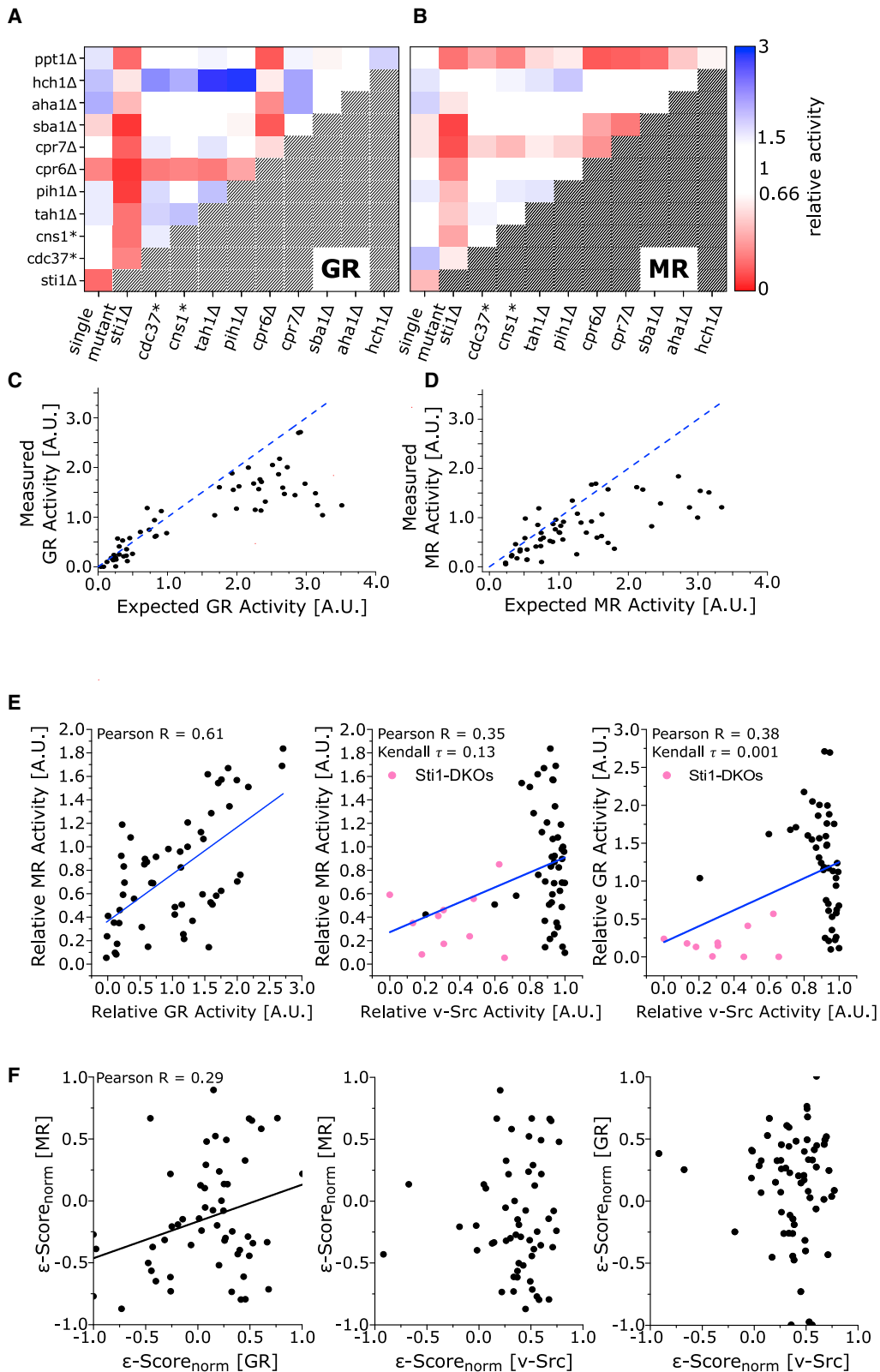
v-Src

The oncogenic kinase v-Src has been used as a reporter of Hsp90 function in yeast in a number of studies due to the robust lethal phenotype (Dey et al., 1996; Goeckeler et al., 2002; Kornbluth et al., 1987; Lee et al., 2002; Montalibet and Kennedy, 2004; Nathan and Lindquist, 1995; Nathan et al., 1999; Panaretou et al., 2002). To investigate the effect of co-chaperones on v-Src kinase activity, v-Src was conditionally expressed in the deletion strains, and v-Src activity was determined via quantifying spot assays (Figure 2A). Our analyses showed that the KO of *STI1* or the KD of *CDC37* significantly increased survival compared to the WT strain, suggesting that Sti1 plays a pivotal role in the maturation of kinases besides the well-established kinase-specific co-chaperone Cdc37, in agreement with previous results (Sahasrabudhe et al., 2017). Interestingly, viability was slightly increased in all other single mutants tested, suggesting that these co-chaperones also modulate the activation of v-Src to some extent. To reveal genetic interactions on the level of client activity, we screened v-Src activity in all co-chaperone double mutants (Figure 2A). More than 90% of the double mutants displayed buffering genetic interactions, indicated by slightly decreased viability, i.e., higher v-Src activity of the double mutant compared to the expected viability (Figure 2B, C). This suggests that most co-chaperones cooperate and form a functional network that aids v-Src maturation. Of note, the strongest positive genetic interactions were evident in strains containing the *cdc37** mutation, confirming the importance of Cdc37 in kinase maturation.

Deletion of *STI1* substantially increased viability in combination with all co-chaperone KOs/KDs tested. Surprisingly, depletion of Cdc37 entailed a much less dominant phenotype and showed the biggest effect in combination with the *cpr7Δ* mutation. Additionally, the KD of Cdc37 increased the viability of *sti1Δ* strain even further. One caveat concerning the *sti1Δ/cdc37** mutant is that *sti1Δ* alone shows considerable viability upon v-Src expression. Hence, the additional depletion of co-chaperones, in particular Cdc37, which also confers a fitness increase in the single mutant, could mask potential negative

Figure 2. v-Src Activity Is Modulated by Hsp90 Co-chaperones

- (A) v-Src activity screen. v-Src kinase was conditionally expressed in yeast and viability of Hsp90 single and double mutants at 30°C was measured by spotting serial dilutions on agar containing 2% D-Galactose (D-Gal). A representative dilution of one biological replicate is shown. The screen was performed in duplicates or triplicates. WT and single-mutant strains were spotted on each plate as control. The density on the D-Gal containing plate was normalized to the growth control on the D-Glc containing plate. The bar chart shows the corrected growth of the mutants relative to the WT. Blue bars indicate WT, red bars indicate single mutants and black bars depict double mutants. Note that the scale for *sti1Δ*- and *cns1**-containing mutants is different from the others.
- (B) Correlation of observed and expected v-Src induced toxicity. The quantified spot density calculated in (A) was used to plot the expected fitness score derived from the multiplied fitness scores of the single mutants correlated with the observed fitness score of the double mutants. Each point represents the average of the two double KO/KD twins (e.g., *sti1Δ/cdc37** and *cdc37*/sti1Δ*).
- (C) ϵ -Score representation of double-mutant fitness with expressed v-Src. The expected and observed growth rates were used to calculate the ϵ -Score. Note that due to the inverse relationship between fitness and v-Src activity, here, the ϵ -Score is defined as $\epsilon = f_a \times f_b - f_{ab}$. The differences between the observed and expected fitness score was normalized to the expected score.
- (D) Sti1 and Cdc37 synergistically promote v-Src activity. Phosphotyrosine levels were quantified in log-phase growing yeast strains expressing v-Src under the GAL1 promoter. Bars represent the means \pm SD of three independent experiments. A representative blot is shown. Significance was evaluated by t testing: n.s., $p \geq 0.05$; * $p \leq 0.05$; ** $p \leq 0.01$; *** $p \leq 0.001$.



(legend on next page)

genetic interactions. To unveil synergism between these co-chaperones in v-Src maturation, we investigated the interplay of Sti1 with Cdc37 in more detail by analyzing their effects on the enzymatic activity of v-Src in yeast. To this end, we measured tyrosine phosphorylation of yeast proteins by v-Src kinase (Brugge et al., 1987; Figure 2D). This assay showed that deletion of *STI1* markedly reduced v-Src activity, as did depletion of Cdc37, but to a smaller degree. Importantly, in the double mutants, tyrosine phosphorylation was almost entirely abolished, confirming a synergistic relationship of these genes on the level of co-chaperone function.

Interestingly, deletion of the *SBA1* gene markedly increased v-Src activity in the *sti1* Δ background (Figure 2A). This positive genetic interaction suggests antagonistic behavior of these co-chaperones during kinase maturation. This is in line with their opposing effect on the Hsp90 conformation (Biebl and Buchner, 2019). Together, these results show that besides the well-established kinase-specific co-chaperone Cdc37, Sti1 also plays a pivotal role in the maturation of v-Src and that the two co-chaperones fulfill partly overlapping functions.

SHRs

To test whether the scenario obtained for the co-chaperone regulation of v-Src activity holds true also for other stringent Hsp90 clients, we determined the activity of the SHRs GR and MR in the single and double co-chaperone mutant strains.

We first evaluated the effects of single mutants on GR and MR activity (Figures 3A and 3B). In agreement with previous studies (Sahasrabudhe et al., 2017), we found that single co-chaperone KOs either decreased or increased GR and MR activity or they did not exhibit an effect. Consistent with the close evolutionary relation between GR and MR, similar patterns of co-chaperone dependence were observed. Yet, some co-chaperones had different effects, suggesting that GR and MR differ in specific requirements of chaperone-assisted maturation. Both GR and MR activity was increased in the *aha1* Δ and *hch1* Δ KO strains and decreased in the *sti1* Δ and *sba1* Δ KO strains, while the other mutants affected the receptors differentially (Figures 3A and 3B). Interestingly, the amplitude of activation and deactivation in the co-chaperone single-mutant strains was smaller for MR than for GR, suggesting that the GR relies more stringently on Hsp90 control.

When we tested for genetic interactions in the co-chaperone double mutants, we found that in ~80% of the double mutants, the activity of the MR or GR was lower than expected, suggesting that most co-chaperones form a genetic interaction network that regulates SHR activity (Figures 3C and 3D). This is in

contrast to what we observed for v-Src, where most co-chaperone double mutants entailed higher activity than what was expected from the single mutants and suggests that the co-chaperones cooperate in different ways for different classes of clients. Importantly, since some single mutants increased SHR activity, the classification of interactions is more complex than for v-Src activity. Interactions could be aggravating if the combined phenotype is more severe than the individual phenotypes. This could either mean lower-than-expected activity if both single mutants had deactivating effects or higher-than-expected activity if the single mutants activated the receptor (Figures S1A and S1B). Interactions were considered buffering if the combined phenotype was less severe than the individual phenotypes. In addition, masking phenotypes were possible if the single mutants had opposing phenotypes (i.e., activating and deactivating) and the combined phenotype deviated from the expected mixed phenotype (Figure S1C). For GR, 24 masking interactions, 28 buffering interactions, and 3 aggravating genetic interactions were detected. In 14 of the 24 masking interactions, the deactivating mutation was dominant, meaning that the activity observed was similar to that of the single KO/KD that reduced receptor activity. By contrast, for MR, we found 32 masking interactions, 14 buffering interactions, and 9 aggravating combinations. Within the pool of masking interactions, in 27 mutants the deactivating mutation had a dominant effect.

When we analyzed the reporter activity in the co-chaperone double mutants, a strong dominant-negative effect on GR activity was obvious in mutants lacking Sti1, Cpr6, and to a lesser extent Sba1/p23, showing that these co-chaperones are pivotal for client maturation (Figure 3A). Additionally, double mutants lacking one of these co-chaperones tended to display lower activity than expected from single KOs. This suggests that these co-chaperones form a core in the network to promote GR maturation. By contrast, the loss of Hch1 usually had a dominant activating effect in the mutants. Interestingly, even though Aha1 is closely related to Hch1 and the KO of *AHA1* and *HCH1* each activate GR, the activating effect of *aha1* Δ seemed to be less dominant and was buffered by the KO of additional co-chaperones. Accordingly, the positive genetic interaction score for *aha1* Δ -containing double mutants was higher than for *hch1* Δ -containing double mutants. Similarly, loss of *STI1* had a dominant-negative effect on MR activity (Figure 3B). The effect of *sba1* Δ was less pronounced and loss of Cpr7, but not Cpr6, had a negative effect on MR activity. This highlights that even closely related clients can have very different co-chaperone requirements for maturation. Additionally, the activating effect of *hch1* Δ and

Figure 3. Hsp90 Clients Are Affected by Client-Specific Co-chaperone Networks

(A and B) GR and MR activity screen. Heatmaps representing the activity of GR (A) and MR (B) in Hsp90 co-chaperone single and double mutants are shown. Red indicates lower activity, blue indicates increased activity compared to WT. Measurements were done in at least four biological replicates and the means of both inherent replicates are depicted.

(C and D) Correlation of the expected with the observed GR (C) and MR (D) activity. The expected receptor activity derived from the multiplied single-mutant activities was correlated with the observed receptor activity. Each point represents one of the double mutants from (A) and (B).

(E) Double-mutant effects on GR, MR and v-Src. The effects of co-chaperone double mutants on GR, MR and v-Src activity were correlated. The Pearson coefficient was calculated for the GR-MR correlation. For the GR-v-Src and MR-v-Src correlation, additionally the Kendall τ -coefficient was calculated. *sti1* Δ -containing double mutants are marked in pink. Each point represents the averaged activity of the double-mutant twins (e.g., *sti1* Δ /*cdc37*⁺ and *cdc37*⁺/*sti1* Δ).

(F) ϵ -Value correlation between GR, MR and v-Src. The normalized ϵ -score of each double mutant was correlated for GR, MR and v-Src. Each point represents the averaged, normalized ϵ -score from the double-mutant twins.

aha1Δ was weaker for MR. Yet, matching the results for GR, the mean genetic interaction score was higher for *aha1Δ*- than for *hch1Δ*-containing mutants. Interestingly, *ppt1Δ* had a dominant-negative effect in most double mutants, while the single mutant did not affect MR activity. This suggests that Ppt1 cooperates with many co-chaperones to promote client maturation and that defects upon Ppt1 deletion only become evident if an additional co-chaperone is lost.

When we analyzed the highest buffering interactions (in which the activity was lower than expected from the single KO activation) in more detail for GR and MR, several of the highest-scoring buffering interactions included the *AHA1* or *HCH1* genes. This strongly suggests that they occupy a central position in the co-chaperone network that mediates GR and MR maturation. Aha1 activates the Hsp90 ATPase, and its KO has previously been shown to positively affect GR and MR activity (Dunn et al., 2015; Harst et al., 2005; Sahasrabudhe et al., 2017). Hch1 is a homolog of Aha1 that is only present in yeast and activates the Hsp90 ATPase slightly (Meyer et al., 2004b; Panaretou et al., 2002). Interestingly, the double KO of *AHA1* and *HCH1* scored highest for GR and second highest for MR, i.e., the SHR activity was considerably lower than expected from the combined effects of the single KOs. In fact, the activity of the *aha1Δ/hch1Δ* double mutant was even lower than the activity of each individual KO, suggesting that the introduction of the second KO alleviated the activating effect of the first KO (Figures 3A and 3B). Thus, Aha1 and Hch1 may act together in a pathway or complex to regulate GR and MR. In summary, GR and MR are subject to specific positive and negative regulation by Hsp90 co-chaperones. There is overlap in the co-chaperone dependence and genetic networks of the two receptors; however, some co-chaperones form genetic interactions that affected activity in a client-specific manner.

Client Specificity of the Co-chaperone Network

To obtain a more general picture of the co-chaperone dependence of the tested clients, we systematically compared how co-chaperone KOs/KDs affected the activities of GR, MR, and v-Src. For the effects of double mutants on GR or MR activity, a Pearson R of 0.61 was calculated, suggesting that the double KOs in general influenced GR and MR activity in a similar way (Figure 3E). Nevertheless, this also indicates that despite the homology and structural similarity between GR and MR, there are significant differences how co-chaperones affect the receptors. This is not due to differences in the overall stability, since GR and MR showed similar degradation kinetics in cycloheximide chase experiments (Figure S4A). The correlation coefficients for either GR or MR activity with v-Src activity were much lower (Figure 3E). This indicates that the double deletions affected SHR activity and kinase activity in markedly different ways. Importantly, the small correlation was due to the shared detrimental effect of the *sti1Δ* on client activity, suggesting that Sti1 had profound impact on the maturation of the unrelated kinase and receptor client classes.

As combinations of KOs/KDs provide information of how co-chaperones cooperate in chaperoning client activity, we compared the genetic interactions between all co-chaperones for GR, MR, and v-Src (Figure 3F). To this end, we correlated

the normalized ϵ -values obtained for GR, MR, and v-Src to obtain information how well the genetic interaction map correlates between the different clients, i.e., how co-chaperones collaborate to ensure client maturation. Surprisingly, we found that the co-chaperone interaction network correlated poorly between GR and MR, with a Pearson R of 0.29, suggesting that the genetic interaction landscape varied markedly between GR and MR. When we compared the ϵ -scores for GR or MR with the scores obtained for v-Src, there was no statistically significant correlation when analyzed with the Pearson, Spearman, or Kendall correlation algorithm. Thus, the active co-chaperome is client specific, and the co-chaperones form different genetic networks to ensure client activation.

Analysis of Specific Epistatic Modules that Affect Client Activity

Epistatic Interactions Affecting Viability

Our viability analysis revealed negative genetic interactions for the double mutants *sti1Δ/cpr7Δ*, *cns1*/cpr7Δ* and *tet07-CNS1/sti1Δ* indicating that Sti1, Cpr7, and Cns1 form a tripartite module, which regulates a common pathway that is required for viability. To gain more insight into the underlying cellular process, we sought to identify the target pathway of this epistatic module. To analyze the genetic interactions between *STI1* and *CPR7* further, we tested their effects on protein translation by ³⁵S-methionine incorporation in logarithmically growing yeast cells (Figure S3B). The *cpr7Δ* strain displayed a significantly reduced protein biosynthesis rate, in agreement with previous results (Schopf et al., 2019; Tenge et al., 2015). Of note, while protein biosynthesis was not affected in the *sti1Δ* strain, the *sti1Δ/cpr7Δ* double KO strain had reduced protein biosynthesis rates (Figure S3B). This suggests that the observed genetic interaction between *CPR7* and *STI1* could be due to their joint involvement in regulating protein biosynthesis. As it was shown recently that eEF2 is chaperoned by the Hsp90 system (Schopf et al., 2019), we determined the aggregation of eEF2 in the *sti1Δ*, *cpr7Δ*, and *sti1Δ/cpr7Δ* strains in comparison to the WT strain. The analyses revealed that eEF2 aggregation is enhanced in the *cpr7Δ* strain and even further increased in the *sti1Δ/cpr7Δ* strain, whereas deletion of *STI1* alone did not significantly affect eEF2 aggregation (Figure S3C). eEF2 showed only a weak tendency toward increased aggregation in the *cns1** mutant (Figure S3C). Yet, introduction of *sti1Δ* into the *cns1** mutant decreased eEF2 solubility, demonstrating the genetic interaction between *CNS1* and *STI1* (Figure S3C). In summary, these findings confirm the genetic interaction for *sti1Δ/cpr7Δ*, *cns1*/cpr7Δ*, and *tet07-CNS1/sti1Δ*, as deduced from our viability screen also for a specific client protein.

v-Src Activation Network

The most striking effect on v-Src activity was observed in mutants lacking Sti1 and Cdc37. To shed light on the regulatory mechanism of the Hsp90 system on v-Src, we performed a cycloheximide chase in the presence of the Hsp90 inhibitor radicicol. Hsp90 inhibition did not lead to increased v-Src degradation in the WT or in the *sti1Δ* and *cdc37** strains in the presence or absence of radicicol (Figures S4B and S4C). Since this suggests a conformational regulation through Hsp90, we tested v-Src solubility. Even in the WT strain, a substantial amount of v-Src was

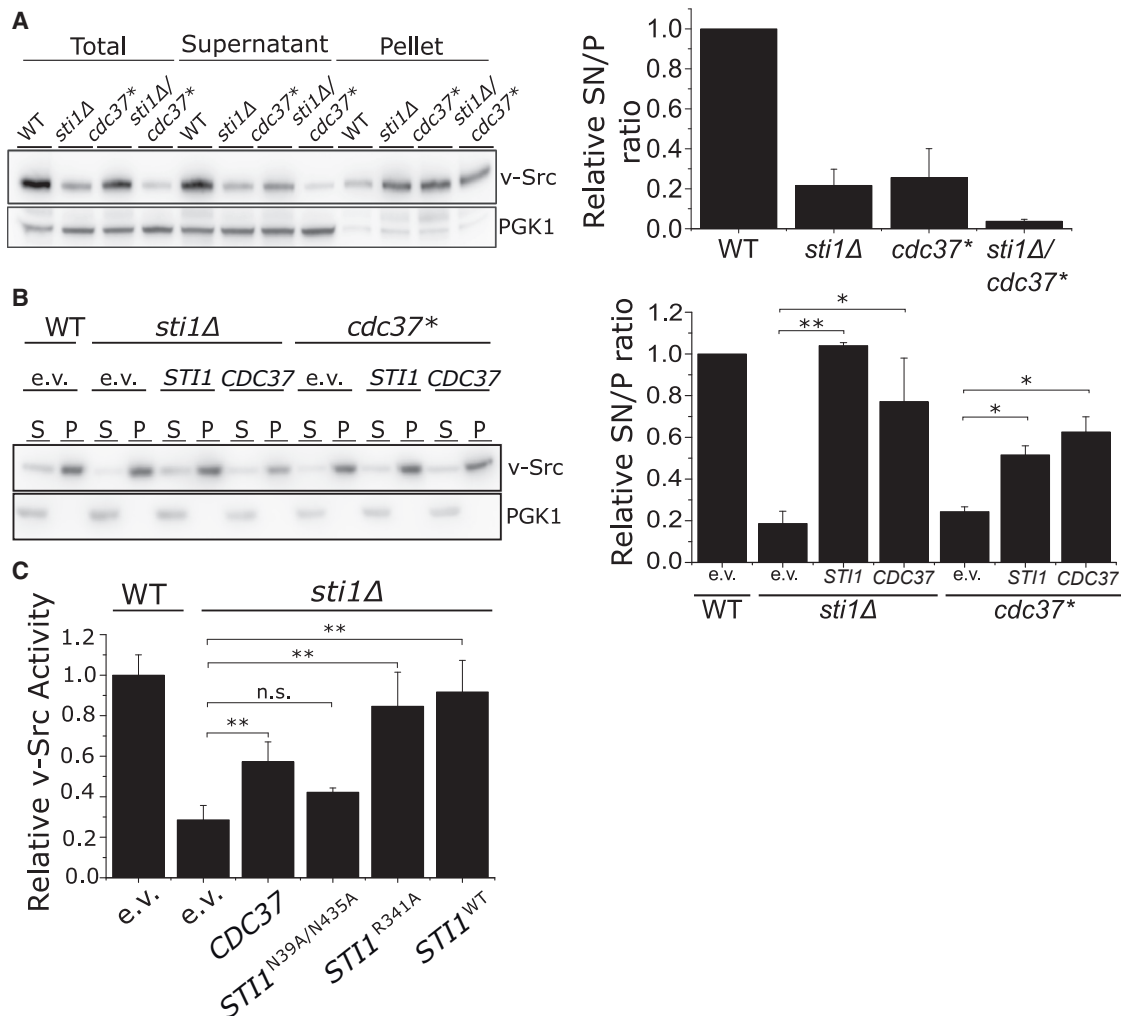


Figure 4. Stt1 and Cdc37 Functionally Overlap in v-Src Maturation

(A) v-Src solubility is maintained by Stt1 and Cdc37. Pellet (P) and supernatant (S) fractions were separated in logarithmically growing yeast cells expressing hemagglutinin (HA)-tagged v-Src. The pellet and supernatant ratios of the mutants were normalized to the WT. P and S levels do not recapitulate cellular ratios but are defined by loading amounts. Bars and error bars represent means \pm SD of three biological replicates.

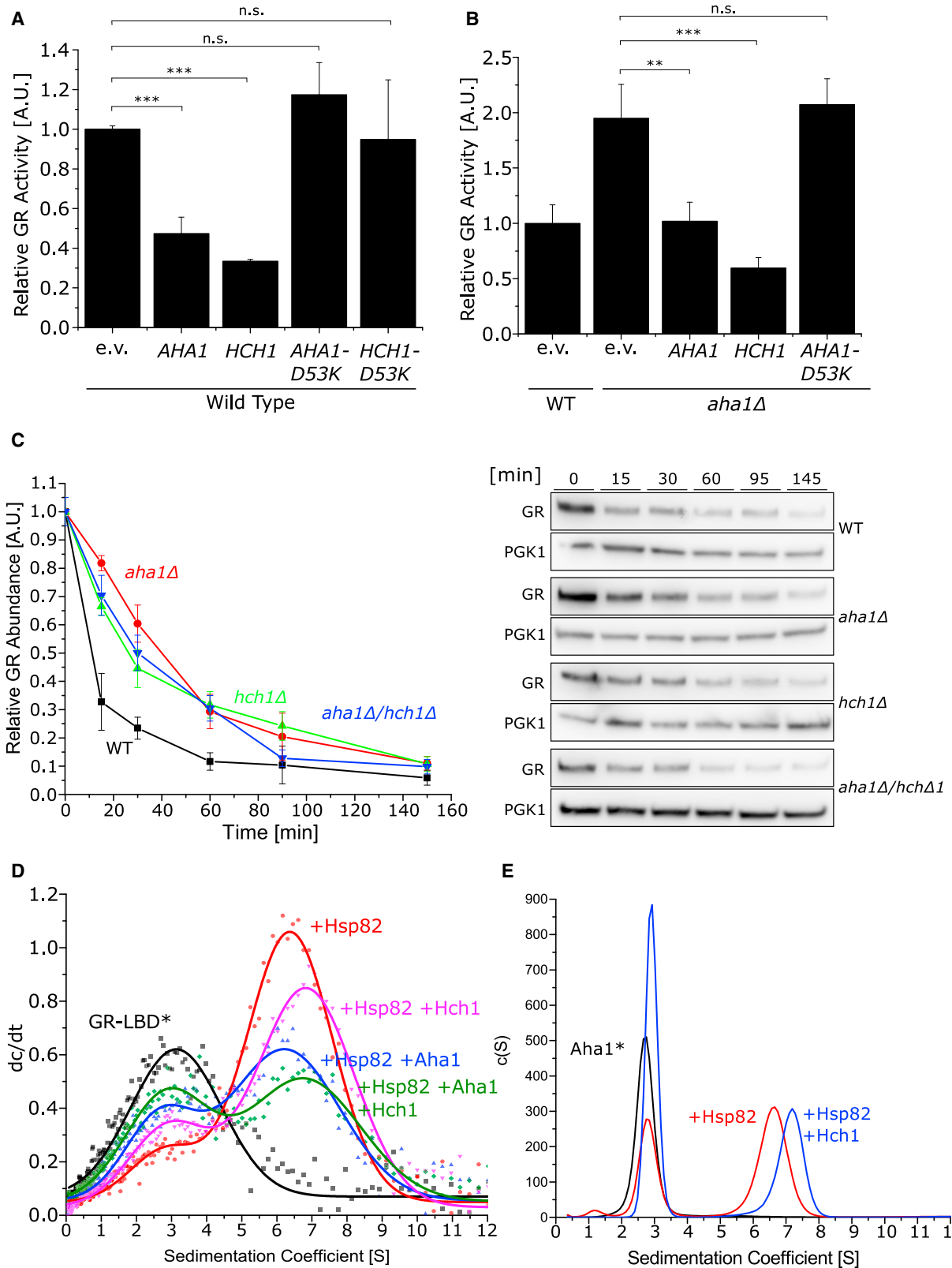
(B) Stt1 and Cdc37 functionally overlap in keeping v-Src soluble. Pellet (P) and supernatant (S) fractions of yeast strains expressing HA-tagged v-Src were separated in the indicated genetic backgrounds expressing either Stt1 or Cdc37 from a plasmid. All ratios were normalized to the WT. P and S fractions do not recapitulate cellular ratios but are defined by the amount that was loaded. Bars represent means \pm SD from two independent biological replicates. e.v. indicates the empty vector control. Significance was evaluated by t testing: n.s., $p \geq 0.05$; * $p \leq 0.05$; ** $p \leq 0.01$; *** $p \leq 0.001$.

(C) Stt1 and Cdc37 have overlapping functions in keeping v-Src active. Phosphotyrosine levels were quantified in yeast strains expressing HA-tagged v-Src and one of the indicated Cdc37 or Stt1 mutants. Bars and errors indicate the means \pm SD of biological triplicates. Significance was determined by t testing: n.s., $p \geq 0.05$; * $p \leq 0.05$; ** $p \leq 0.01$; *** $p \leq 0.001$.

found in the pellet fraction. Solubility was considerably more compromised in the *sti1Δ* (~80% reduction), *cdc37** (~75% reduction) single mutants and the *sti1Δ/cdc37** (~95% reduction) double mutant (Figure 4A). Thus, both co-chaperones are involved in maintaining the native fold of v-Src. To test whether the surprisingly central role of Stt1 in maintaining kinase function is restricted to v-Src, we tested its effect on the endogenous yeast kinase Ste11, which regulates yeast mating and leads to growth arrest in the presence of inducing pheromone (Louvion et al., 1998). We used the constitutively active Δ N-Ste11 mutant (Louvion et al., 1998), which lacks a regulatory domain and led to

a partial growth arrest in yeast (Figure S5). Notably, when we monitored the effects of *STI1* KO or depletion of Cdc37, we found that the growth defect induced by Δ N-Ste11 was rescued. These results confirm that Stt1 and Cdc37 are also important for the maturation of an endogenous yeast client kinase.

Since synergism between genes suggests parallel pathways, we tested whether Cdc37 and Stt1 could rescue the loss of each other. To this end, we expressed Stt1 or Cdc37 from a plasmid in a KO/KD strain of the respective other co-chaperone and tested for v-Src solubility (Figure 4B). These experiments showed that Stt1 can compensate for the loss of Cdc37 and



(legend on next page)

vice versa confirming the hypothesis that Sti1 and Cdc37 act in parallel pathways. Importantly, also on the activity level, Cdc37 was able to rescue the loss of Sti1 (Figure 4C). Sti1 acts as an adaptor protein that connects the Hsp70 system to the Hsp90 system by tetratricopeptide repeat (TPR) domains that can bind the C-terminal EEVD motifs of Hsp70 and Hsp90 (Chen and Smith, 1998; Johnson et al., 1998; Röhl et al., 2015; Scheufler et al., 2000; Schmid et al., 2012). Hence, Sti1 promotes client handover from Hsp70 to Hsp90. By contrast, Cdc37 is a kinase-specific recruiter co-chaperone that directly binds Hsp90. To test the relevance of the Hsp70 system in this context, we tested the Sti1^{N39A/N435A} mutant that is compromised in Hsp70 binding (Röhl et al., 2015). We found that this mutant could not rescue the loss of Sti1 (Figure 4C), indicating that the observed effects of Sti1 on v-Src activity are caused by the bridging between Hsp40/70 and Hsp90 and not only by the effect of Sti1 on Hsp90 conformation and ATPase. Consequently, we hypothesize that v-Src is trapped in the Hsp70 system in the absence of Sti1 and therefore cannot reach its functional state. Together, these results reveal overlapping functions of Sti1 and Cdc37 in v-Src maturation and that the release of v-Src from Hsp70 is pivotal for activation. Hence, partially parallel pathways for kinase recruitment to Hsp90 by Cdc37 or Hsp70:Sti1 seem to have evolved.

SHR Activation Network

The most significant genetic interaction our screen revealed was the buffering behavior of the *aha1Δ* and *hch1Δ* mutations that were conserved between GR and MR. To analyze the role of Aha1 and Hch1 in the GR maturation process in more detail, we checked whether overexpression of Aha1 and Hch1 in WT cells could decrease GR activity. Overexpression significantly reduced the activity of GR and this effect was dependent on Aha1 and Hch1 binding to Hsp90, since overexpression of the binding-deficient mutants Aha1^{D53K} and Hch1^{D53K} did not affect GR activity (Figure 5A). Furthermore, in the *aha1Δ* strain, overexpression of Aha1, but not Aha1^{D53K}, reversed the effect of the *aha1Δ* mutation (Figure 5B). Overexpression of Hch1 even reduced the activity further in the *aha1Δ* background, suggesting that Hch1 can functionally replace Aha1 in this reaction. Yet, functional differences are obvious, considering that Hch1, but not Aha1, was able to partially rescue the detrimental effects of the *STI1*, *CPR6*, or *SBA1* KOs.

We then analyzed how the *aha1Δ*, *hch1Δ* or the combined *aha1Δ/hch1Δ* mutation affected GR stability *in vivo* by following GR levels after cycloheximide treatment (Figure 5C). In all mutants, GR degradation was delayed 2- to 3-fold compared to

the WT, suggesting that loss of Aha1 and Hch1 stabilized GR, but the stabilizing effect was not additive or synergistic when both co-chaperones were missing, which matches the activity data. To determine how Aha1 and Hch1 affect client binding to Hsp90, we turned to *in vitro* experiments studying complex formation by analytical ultracentrifugation. The labeled GR ligand-binding domain (GR-LBD[#]) efficiently bound yeast Hsp82 in the presence of ATP-γS (Figure 5D). When Aha1 or Hch1 was added, the GR-LBD[#] was displaced in agreement with previous studies (Lorenz et al., 2014; Sahasrabudhe et al., 2017). Of note, a ternary complex between the GR-LBD[#], Hsp90 and Hch1 could be formed, while Aha1 could not bind together with the GR-LBD[#] to Hsp90. This suggests differences in binding which may account for the mentioned functional differences between Aha1 and Hch1. Although Aha1 and Hch1 compete for binding to Hsp90, a trimeric Hsp90:Aha1:Hch1 complex exists, confirming the idea of different binding modes (Figure 5E). Together with the *in vivo* activity data, this suggests that the increased dwell time of GR on Hsp90 in the *aha1Δ* and *hch1Δ* KO strains leads to an increased GR activity. Yet, further extension of the time bound to Hsp90 by the simultaneous KO of *AHA1* and *HCH1* did not increase activity.

DISCUSSION

Despite extensive research on the Hsp90 chaperone machinery, surprisingly little is known about how co-chaperones affect client maturation *in vivo* and whether they cooperate. Genetic interaction data from large-scale synthetic genetic array screens of recent years provide a tremendous resource to delineate protein complexes and pathways (Kuzmin et al., 2018; Rizzolo et al., 2017, 2018; Zhao et al., 2005). However, as fitness was used as the readout, they do not necessarily provide insight into how genes interact for executing a specific function like maturation of a given Hsp90 client.

In line with these general studies, we could show that synthetic lethality was absent between Hsp90 co-chaperones and that only a few double mutants displayed negative fitness. Also most combinations of two co-chaperones can be lost without obvious growth phenotypes. This suggests that co-chaperones may have individual functions and thus fine-tune the Hsp90 machinery.

When we screened the activity of specific clients (v-Src, GR, and MR) in all double-mutant backgrounds, we found a surprising central role of Sti1 in the maturation process of v-Src (Figures 6A and 6B) and a negative genetic interaction between Sti1 and Cdc37, suggesting that these co-chaperones may have

Figure 5. Aha1 and Hch1 Regulate GR Binding to Hsp90

(A) Overexpression of Aha1 and Hch1 reduce GR activity. Aha1, Hch1, or the Hsp90-binding-deficient Aha1^{D53K} and Hch1^{D53K} mutants were overexpressed in yeast strains co-expressing the GR and the reporter plasmid. Bars indicate the means ± SD of at least four biological replicates. Significance was evaluated by t testing: n.s., p ≥ 0.05; *p ≤ 0.05; **p ≤ 0.01; ***p ≤ 0.001.

(B) Overexpression of Aha1 and Hch1 rescue the loss of Aha1. Aha1, Hch1, or the Aha1^{D53K} mutant were co-expressed with GR and the reporter plasmid in the *aha1Δ* background. Bars indicate the means ± SD of at least four biological replicates. Significance was calculated by t testing: n.s., p ≥ 0.05; *p ≤ 0.05; **p ≤ 0.01; ***p ≤ 0.001.

(C) Loss of Aha1 or Hch1 reduces GR degradation. The levels of HA-tagged GR were monitored in the indicated mutants after protein expression was inhibited by the addition of cycloheximide. Shown are the means ± SD of biological triplicates.

(D) Aha1 and Hch1 displace GR from Hsp90. Aha1 (3 μM) and Hch1 (3 μM) were added to Hsp82:GR-LBD[#] complexes in analytical ultracentrifugation experiments. Hsp82 was used at a dimer concentration of 1.5 μM, and GR-LBD[#] was used at a concentration of 500 nM.

(E) Aha1 and Hch1 compete for Hsp90 binding. Aha1[#] (500 nM) and Hch1 (6 μM) binding to Hsp90 (2.5 μM dimer) was tested by analytical ultracentrifugation.

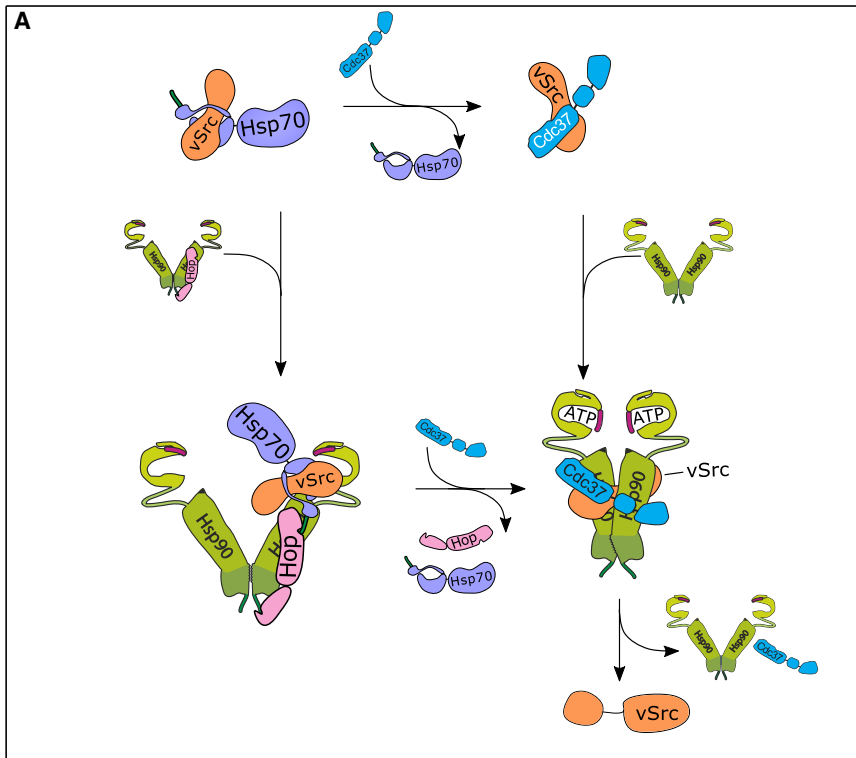
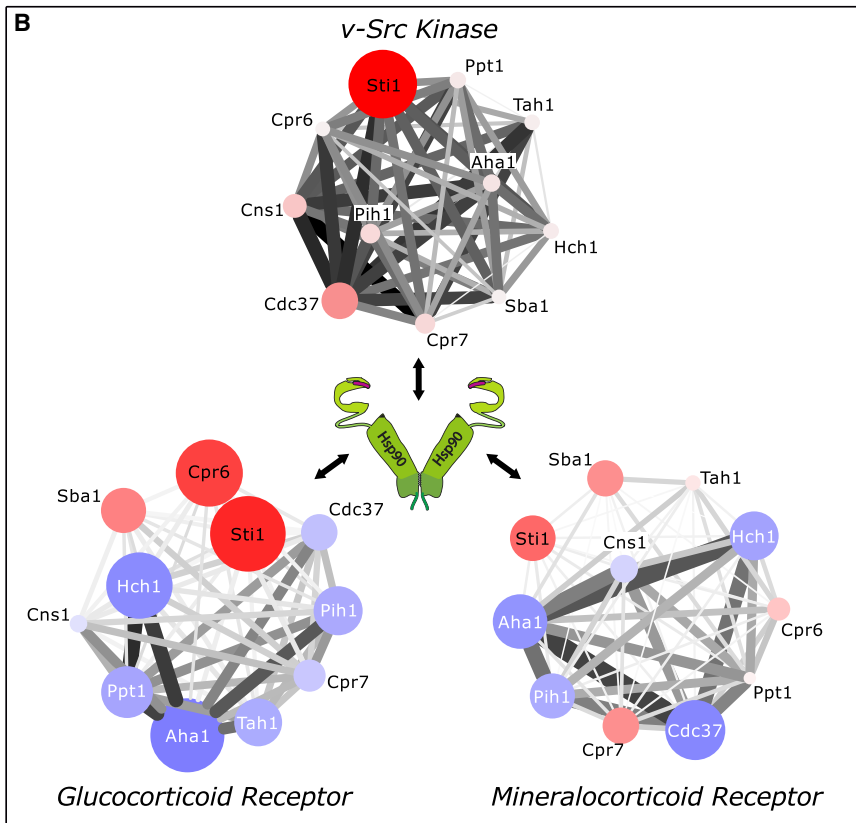


Figure 6. Different Genetic Interaction Networks Are Required for Different Clients

(A) Schematic model depicting partially parallel pathways of Cdc37 and Sti1 in kinase maturation. Hsp70 and Cdc37 have overlapping functions by stabilizing partially unfolded client states. While Cdc37 can stabilize a kinase and recruit it to Hsp90, Hsp70 requires Sti1 for the transfer. In both pathways, Cdc37 can bind the Hsp90:kinase complex to promote maturation.

(B) Schematic model showing client-specific co-chaperone networks. Co-chaperones are depicted as circles and are color-coded with respect to their effect on client maturation (red, KO/KD is deactivating; blue, KO/KD is activating). The size of the circle and the saturation representative the magnitude of their effects. Genetic interactions between co-chaperones are shown as edges; edge size and saturation of color indicate the strength of the interaction (white, weak; black, strong).



compensatory roles in parallel pathways. This is in line with previous findings that established a genetic and physical interaction of Cdc37 mutants and Sti1 on the level of growth fitness (Abbas-Terki et al., 2002). Accordingly, the overexpression of Sti1 and Cdc37 compensated the effects of depleting CDC37 or the loss of STI1 on v-Src aggregation and activity, respectively. Sti1 is important for the transfer of client proteins from Hsp70 to Hsp90 (Chen and Smith, 1998; Johnson et al., 1998; Röhl et al., 2015; Schmid et al., 2012), and Cdc37 has been shown to act as a kinase-specific recruiter co-chaperone (Citri et al., 2006; Grammatikakis et al., 1999; Keramisanou et al., 2016; Kimura et al., 1997). Thus, these results indicate that at least for some kinases, Sti1 may be able to replace the function of Cdc37. Our results also suggest that the Hsp70 system plays an important role in kinase activation and that specifically the release of kinases from Hsp70 is a decisive step, in line with previous results (Moran Luengo et al., 2018). Specifically, we found that the main function of Sti1 for v-Src activation is its ability to bridge Hsp70 and Hsp90 and not the conformational influence it has on Hsp90. This conclusion was drawn from testing the effect of a Sti1 mutant lacking the ability to bind Hsp70, which could not rescue the loss of Sti1. Studies in the mammalian system, which found that Cdc37 can exert mild unfolding pressure on kinases (Keramisanou et al., 2016) and that binding of clients to Hsp70 leads to the partial unfolding of clients (Boysen et al., 2019; Dahiya et al., 2019; Kirschke et al., 2014; Moran Luengo et al., 2018), support overlapping roles of Cdc37 and Sti1:Hsp70. Importantly, these roles for Cdc37 and Sti1/Hop and Hsp70 seem to be conserved, since they have been observed in the yeast, mammalian, and mixed systems (Boysen et al., 2019; Dahiya et al., 2019; Keramisanou et al., 2016; Kirschke et al., 2014; Moran Luengo et al., 2018).

Of note, both co-chaperones evidently have distinct functions, since CDC37, but not STI1, is essential. Furthermore, their interaction with Hsp90 is strikingly different. While Sti1 binds to the open state of Hsp90 and blocks the ATPase as a noncompetitive inhibitor (Prodromou et al., 1999; Richter et al., 2003; Schmid et al., 2012), Cdc37 binds to the closed state and inhibits the ATPase partially (Eckl et al., 2013; Roe et al., 2004; Siligardi et al., 2002; Verba et al., 2016).

Hence, we propose a model, in which two partially parallel pathways have evolved to keep v-Src in a partially unfolded state and guiding it to Hsp90 (Figure 6A). While Cdc37 can perform both functions, Hsp70 requires Sti1 to promote kinase transfer to Hsp90. Consistent with the structure of the Hsp90:Cdc37:Cdk4 kinase complex (Verba et al., 2016), Cdc37 could form a Hsp90:kinase:Cdc37 complex after client transfer of the kinase from Hsp70 to Hsp90. Parallel pathways may be beneficial to increase the repertoire of v-Src conformations that can be trapped and funneled toward the Hsp90 machinery.

We also found a buffering genetic interaction between Sti1 and Sba1/p23, suggesting that these co-chaperones are part of a linear pathway, which is in line with the model that p23 acts late in the Hsp90 cycle, whereas Sti1 acts early in the cycle. Possibly, Sba1/p23 forms an Hsp90:kinase:p23 complex that is preceded by a Hsp90:Sti1:kinase complex.

Finally, the v-Src activity screen revealed that besides a few co-chaperones that displayed a strong effect on client activity, all co-

chaperones tested had a weak to modest positive effect, suggesting that besides a core set of important co-chaperones, the entire co-chaperome participates in fine-tuning kinase maturation.

Interestingly, when we tested SHRs, ~85% of the double mutants displayed lower activity than expected from the single KOs/KDs, which is different from the situation for v-Src, where activity was increased in most double mutants. However, these results match early studies from the Lindquist lab, where opposing effects on SHRs and v-Src were observed when the Hsp40/70-Hsp90 system was perturbed (Kimura et al., 1995). We envision that mechanistic differences in the maturation process of kinases and SHRs are reflected in the differences in the co-chaperone requirement of SHRs versus kinases. In particular, we found that Hsp90 inhibition leads to the rapid degradation of SHRs, but not of v-Src. Additionally, despite overlapping binding sites on Hsp90, current evidence suggests that the binding modes of kinases and SHRs are different (Lorenz et al., 2014; Verba et al., 2016). While the GR-LBD was shown to bind to the outside of N-terminally dimerized Hsp90 (Lorenz et al., 2014), the N-lobe and C-lobe of the kinase Cdk4 are separated and the connecting stretch is threaded through an orifice in the Hsp90 dimer (Verba et al., 2016). Hence, Hsp90 interaction imparts dramatic conformational changes on kinases. For GR, conformational plasticity is functionally important (Suren et al., 2018). Hsp90 is thought to prevent the unfolding of a small loop that holds the hormone in place (Suren et al., 2018). Hence, the requirements for conformational processing seem to be different between SHRs and kinases, and it is tempting to speculate that the different nature of genetic interactions of GR/MR and v-Src are a product of these differences.

The accelerators Aha1 and Hch1, which led to increased GR and MR activity when individually knocked out, surprisingly, displayed a strong buffering genetic interaction when deleted together (Figure 6B). Both effectively displaced GR from an Hsp90:GR complex, suggesting that they regulate the dwell time of GR on Hsp90. This is consistent with overlapping binding sites for Aha1 and the GR-LBD (Lorenz et al., 2014), and the finding that the knockdown of Aha1 in mammalian cells could rescue CFTR F508 Δ , supposedly by increasing the dwell time on Hsp90 (Wang et al., 2006). In humans, Hch1 is not present and it has been suggested that a post-translational modification on Tyr627 of human Hsp90 functionally replaces Hch1 (Zuehlke et al., 2017). This may enable a more rapid and more flexible regulation of client binding to Hsp90. Regulating the dwell time of specific clients by co-chaperones may allow to maintain a pool of Hsp90 molecules in an acceptor state for clients or to limit the activation of certain clients.

In general, our results show that the Hsp90 co-chaperone system in yeast is robust and that the co-chaperones are functionally independent units concerning the maintenance of viability. In most cases, the loss of two co-chaperones did not lead to a breakdown of client maturation. Of note, those double mutants that do have pronounced effects were client specific. No double mutant led to the breakdown of chaperone function across different clients. The structurally related GR and MR exhibit some overlap in their dependence on co-chaperones, while negligible overlap was found with v-Src (Figure 6B). Differences between clients were also evident from the genetic interaction

scores, showing that the co-chaperones cooperate in different ways for different clients to support their maturation (Figure 6B). Hence, not only the co-chaperone dependence but also the interaction networks of the co-chaperones are client specific. Notably, some new co-chaperones, such as tuberous sclerosis complex 1 (Tsc1) or Folliculin-interacting protein 1/2 (FNIP1/2), emerged in mammals and have also been shown to affect kinases and SHRs (Woodford et al., 2016, 2017). This suggests that the general co-chaperone network complexity increased further from yeast to mammals. Differences in co-chaperone effects on closely related SHRs have also been reported for mammalian cells (Cox et al., 2007; Riggs et al., 2003; Storer et al., 2011). Based on the similarities of modules in the yeast and the human Hsp90 co-chaperone system, we assume that the basic genetic interactions within the Hsp90 machinery are conserved from yeast to humans.

Together, our study provides a comprehensive view of co-chaperone epistasis during client maturation in yeast. The picture emerging from this analysis is that of a chaperone system that is robust against the loss of components. To promote client maturation, co-chaperones do not act independently but form small epistatic modules embedded in client-specific flexible genetic networks of weak genetic interactions (Figure 6B) that render Hsp90 a plastic modular machinery that adapts to the requirements of each client via different co-chaperone teams.

STAR★METHODS

Detailed methods are provided in the online version of this paper and include the following:

- KEY RESOURCES TABLE
- RESOURCE AVAILABILITY
 - Lead Contact
 - Materials Availability
 - Data and Code Availability
- EXPERIMENTAL MODEL AND SUBJECT DETAILS
- METHOD DETAILS
 - Yeast Transformation
 - Generation of Yeast Strains
 - SEM
 - SHR Activity Screening
 - Viability Screening
 - v-Src Activity Screening
 - Ste11 Activity Analysis
 - Phosphotyrosine Kinase Activity Measurements
 - Aggregate Isolation
 - Cycloheximide Chase
 - Protein Expression and Purification
 - Analytical Ultracentrifugation
 - ³⁵S-Methionine Incorporation
 - Genetic Interactions
- QUANTIFICATION AND STATISTICAL ANALYSIS

SUPPLEMENTAL INFORMATION

Supplemental Information can be found online at <https://doi.org/10.1016/j.celrep.2020.108063>.

ACKNOWLEDGMENTS

This work was performed within the framework of SFB 1035 (German Research Foundation [DFG], Sonderforschungsbereich 1035, Projektnummer 201302640, project A03). M.M.B. was supported by a scholarship of the Fonds der chemischen Industrie. We thank Bettina Richter, Daniel Rutz, Christopher Dodt, and Florian Schopf for experimental help and advice.

AUTHOR CONTRIBUTIONS

M.M.B. performed experiments and analyses. M.R. helped with experiments and analyses. M.M.B. and J.B. wrote the paper.

DECLARATION OF INTERESTS

The authors declare no competing interests.

Received: February 19, 2020

Revised: July 1, 2020

Accepted: August 3, 2020

Published: August 25, 2020

REFERENCES

- Abbas-Terki, T., Donzé, O., and Picard, D. (2000). The molecular chaperone Cdc37 is required for Ste11 function and pheromone-induced cell cycle arrest. *FEBS Lett.* 467, 111–116.
- Abbas-Terki, T., Briand, P.A., Donzé, O., and Picard, D. (2002). The Hsp90 co-chaperones Cdc37 and Sti1 interact physically and genetically. *Biol. Chem.* 383, 1335–1342.
- Ali, M.M., Roe, S.M., Vaughan, C.K., Meyer, P., Panaretou, B., Piper, P.W., Prodromou, C., and Pearl, L.H. (2006). Crystal structure of an Hsp90-nucleotide-p23/Sba1 closed chaperone complex. *Nature* 440, 1013–1017.
- Baerends, R.J., Faber, K.N., Kram, A.M., Kiel, J.A., van der Klei, I.J., and Veenhuis, M. (2000). A stretch of positively charged amino acids at the N terminus of *Hansenula polymorpha* Pex3p is involved in incorporation of the protein into the peroxisomal membrane. *J. Biol. Chem.* 275, 9986–9995.
- Ben-David, U., Siranosian, B., Ha, G., Tang, H., Oren, Y., Hinohara, K., Strathdee, C.A., Dempster, J., Lyons, N.J., Burns, R., et al. (2018). Genetic and transcriptional evolution alters cancer cell line drug response. *Nature* 560, 325–330.
- Biebl, M.M., and Buchner, J. (2019). Structure, function, and regulation of the Hsp90 machinery. *Cold Spring Harb. Perspect. Biol.* 11, a034017.
- Boczek, E.E., Reefschläger, L.G., Dehling, M., Struller, T.J., Häusler, E., Seidl, A., Kaila, V.R., and Buchner, J. (2015). Conformational processing of oncogenic v-Src kinase by the molecular chaperone Hsp90. *Proc. Natl. Acad. Sci. USA* 112, E3189–E3198.
- Bohen, S.P., and Yamamoto, K.R. (1993). Isolation of Hsp90 mutants by screening for decreased steroid receptor function. *Proc. Natl. Acad. Sci. USA* 90, 11424–11428.
- Bose, S., Weigl, T., Bügl, H., and Buchner, J. (1996). Chaperone function of Hsp90-associated proteins. *Science* 274, 1715–1717.
- Boysen, M., Kityk, R., and Mayer, M.P. (2019). Hsp70- and Hsp90-mediated regulation of the conformation of p53 DNA binding domain and p53 cancer variants. *Mol. Cell* 74, 831–843.e834.
- Brugge, J.S., Jarosik, G., Andersen, J., Queral-Lustig, A., Fedor-Chaikin, M., and Broach, J.R. (1987). Expression of Rous sarcoma virus transforming protein pp60v-src in *Saccharomyces cerevisiae* cells. *Mol. Cell. Biol.* 7, 2180–2187.
- Chang, H.C., and Lindquist, S. (1994). Conservation of Hsp90 macromolecular complexes in *Saccharomyces cerevisiae*. *J. Biol. Chem.* 269, 24983–24988.
- Chen, S., and Smith, D.F. (1998). Hop as an adaptor in the heat shock protein 70 (Hsp70) and hsp90 chaperone machinery. *J. Biol. Chem.* 273, 35194–35200.

- Citri, A., Harari, D., Shohat, G., Ramakrishnan, P., Gan, J., Lavi, S., Eisenstein, M., Kimchi, A., Wallach, D., Pietrovski, S., and Yarden, Y. (2006). Hsp90 recognizes a common surface on client kinases. *J. Biol. Chem.* *281*, 14361–14369.
- Collins, S.R., Miller, K.M., Maas, N.L., Roguev, A., Fillingham, J., Chu, C.S., Schuldiner, M., Gebbia, M., Recht, J., Shales, M., et al. (2007). Functional dissection of protein complexes involved in yeast chromosome biology using a genetic interaction map. *Nature* *446*, 806–810.
- Costanzo, M., VanderSluis, B., Koch, E.N., Baryshnikova, A., Pons, C., Tan, G., Wang, W., Usaj, M., Hanchard, J., Lee, S.D., et al. (2016). A global genetic interaction network maps a wiring diagram of cellular function. *Science* *353*, 353.
- Cox, M.B., and Johnson, J.L. (2018). Evidence for Hsp90 co-chaperones in regulating Hsp90 function and promoting client protein folding. *Methods Mol. Biol.* *1709*, 397–422.
- Cox, M.B., Riggs, D.L., Hessling, M., Schumacher, F., Buchner, J., and Smith, D.F. (2007). FK506-binding protein 52 phosphorylation: a potential mechanism for regulating steroid hormone receptor activity. *Mol. Endocrinol.* *21*, 2956–2967.
- Dahiya, V., Agam, G., Lawatscheck, J., Rutz, D.A., Lamb, D.C., and Buchner, J. (2019). Coordinated conformational processing of the tumor suppressor protein p53 by the Hsp70 and Hsp90 chaperone machineries. *Mol. Cell* *74*, 816–830.e817.
- Deutschbauer, A.M., Jaramillo, D.F., Proctor, M., Kumm, J., Hillenmeyer, M.E., Davis, R.W., Nislow, C., and Giaever, G. (2005). Mechanisms of haploinsufficiency revealed by genome-wide profiling in yeast. *Genetics* *169*, 1915–1925.
- Dey, B., Caplan, A.J., and Boschelli, F. (1996). The Ydj1 molecular chaperone facilitates formation of active p60v-src in yeast. *Mol. Biol. Cell* *7*, 91–100.
- Dittmar, K.D., Hutchison, K.A., Owens-Grillo, J.K., and Pratt, W.B. (1996). Reconstitution of the steroid receptor.hsp90 heterocomplex assembly system of rabbit reticulocyte lysate. *J. Biol. Chem.* *271*, 12833–12839.
- Duina, A.A., Chang, H.C., Marsh, J.A., Lindquist, S., and Gaber, R.F. (1996a). A cyclophilin function in Hsp90-dependent signal transduction. *Science* *274*, 1713–1715.
- Duina, A.A., Marsh, J.A., and Gaber, R.F. (1996b). Identification of two Cyp-40-like cyclophilins in *Saccharomyces cerevisiae*, one of which is required for normal growth. *Yeast* *12*, 943–952.
- Dunn, D.M., Woodford, M.R., Truman, A.W., Jensen, S.M., Schulman, J., Caza, T., Remillard, T.C., Loisele, D., Wolfgeher, D., Blagg, B.S., et al. (2015). c-Abl mediated tyrosine phosphorylation of Aha1 activates its co-chaperone function in cancer cells. *Cell Rep.* *12*, 1006–1018.
- Echeverría, P.C., Bernthaler, A., Dupuis, P., Mayer, B., and Picard, D. (2011). An interaction network predicted from public data as a discovery tool: application to the Hsp90 molecular chaperone machine. *PLoS ONE* *6*, e26044.
- Echtenkamp, F.J., Gvozdenov, Z., Adkins, N.L., Zhang, Y., Lynch-Day, M., Watanabe, S., Peterson, C.L., and Freeman, B.C. (2016). Hsp90 and p23 molecular chaperones control chromatin architecture by maintaining the functional pool of the RSC chromatin remodeler. *Mol. Cell* *64*, 888–899.
- Eckert, K., Saliou, J.M., Monlezun, L., Vigouroux, A., Atmane, N., Caillaud, C., Quevillon-Chéruef, S., Madiona, K., Nicaise, M., Lazereg, S., et al. (2010). The Pih1-Tah1 co-chaperone complex inhibits Hsp90 molecular chaperone ATPase activity. *J. Biol. Chem.* *285*, 31304–31312.
- Eckl, J.M., Rutz, D.A., Haslbeck, V., Zierer, B.K., Reinstein, J., and Richter, K. (2013). Cdc37 (cell division cycle 37) restricts Hsp90 (heat shock protein 90) motility by interaction with N-terminal and middle domain binding sites. *J. Biol. Chem.* *288*, 16032–16042.
- Elena, S.F., and Lenski, R.E. (1997). Test of synergistic interactions among deleterious mutations in bacteria. *Nature* *390*, 395–398.
- Esposito, A.M., and Kinzy, T.G. (2014). In vivo [35S]-methionine incorporation. *Methods Enzymol.* *536*, 55–64.
- Fang, Y., Fliss, A.E., Robins, D.M., and Caplan, A.J. (1996). Hsp90 regulates androgen receptor hormone binding affinity in vivo. *J. Biol. Chem.* *271*, 28697–28702.
- Frattini, A., Fabbri, M., Valli, R., De Paoli, E., Montalbano, G., Gribaldo, L., Pasquali, F., and Maserati, E. (2015). High variability of genomic instability and gene expression profiling in different HeLa clones. *Sci. Rep.* *5*, 15377.
- Freeman, B.C., Toft, D.O., and Morimoto, R.I. (1996). Molecular chaperone machines: chaperone activities of the cyclophilin Cyp-40 and the steroid aporeceptor-associated protein p23. *Science* *274*, 1718–1720.
- Genest, O., Reidy, M., Street, T.O., Hoskins, J.R., Camberg, J.L., Agard, D.A., Masion, D.C., and Wickner, S. (2013). Uncovering a region of heat shock protein 90 important for client binding in *E. coli* and chaperone function in yeast. *Mol. Cell* *49*, 464–473.
- Gietz, R.D., and Schiestl, R.H. (2007). High-efficiency yeast transformation using the LiAc/SS carrier DNA/PEG method. *Nat. Protoc.* *2*, 31–34.
- Goeckeler, J.L., Stephens, A., Lee, P., Caplan, A.J., and Brodsky, J.L. (2002). Overexpression of yeast Hsp110 homolog Sse1p suppresses ydj1-151 thermosensitivity and restores Hsp90-dependent activity. *Mol. Biol. Cell* *13*, 2760–2770.
- Grammatikakis, N., Lin, J.H., Grammatikakis, A., Tschlis, P.N., and Cochran, B.H. (1999). p50(cdc37) acting in concert with Hsp90 is required for Raf-1 function. *Mol. Cell. Biol.* *19*, 1661–1672.
- Harst, A., Lin, H., and Obermann, W.M. (2005). Aha1 competes with Hop, p50 and p23 for binding to the molecular chaperone Hsp90 and contributes to kinase and hormone receptor activation. *Biochem. J.* *387*, 789–796.
- Hayes, D.B., and Stafford, W.F. (2010). SEDVIEW, real-time sedimentation analysis. *Macromol. Biosci.* *10*, 731–735.
- Jakob, U., Lilie, H., Meyer, I., and Buchner, J. (1995). Transient interaction of Hsp90 with early unfolding intermediates of citrate synthase. Implications for heat shock in vivo. *J. Biol. Chem.* *270*, 7288–7294.
- Janke, C., Magiera, M.M., Rathfelder, N., Taxis, C., Reber, S., Maekawa, H., Moreno-Borchart, A., Doenges, G., Schwob, E., Schiebel, E., and Knop, M. (2004). A versatile toolbox for PCR-based tagging of yeast genes: new fluorescent proteins, more markers and promoter substitution cassettes. *Yeast* *21*, 947–962.
- Johnson, J.L. (2012). Evolution and function of diverse Hsp90 homologs and cochaperone proteins. *Biochim. Biophys. Acta* *1823*, 607–613.
- Johnson, J.L., and Brown, C. (2009). Plasticity of the Hsp90 chaperone machine in divergent eukaryotic organisms. *Cell Stress Chaperones* *14*, 83–94.
- Johnson, B.D., Schumacher, R.J., Ross, E.D., and Toft, D.O. (1998). Hop modulates Hsp70/Hsp90 interactions in protein folding. *J. Biol. Chem.* *273*, 3679–3686.
- Johnson, J.L., Zuehlke, A.D., Tenge, V.R., and Langworthy, J.C. (2014). Mutation of essential Hsp90 co-chaperones SGT1 or CNS1 renders yeast hypersensitive to overexpression of other co-chaperones. *Curr. Genet.* *60*, 265–276.
- Joshi, S., Wang, T., Araujo, T.L.S., Sharma, S., Brodsky, J.L., and Chiosis, G. (2018). Adapting to stress - chaperome networks in cancer. *Nat. Rev. Cancer* *18*, 562–575.
- Keramisanou, D., Aboalroub, A., Zhang, Z., Liu, W., Marshall, D., Divinye, A., Larsen, R.W., Landgraf, R., and Gelis, I. (2016). Molecular mechanism of protein kinase recognition and sorting by the Hsp90 kinome-specific cochaperone Cdc37. *Mol. Cell* *62*, 260–271.
- Kimura, Y., Yahara, I., and Lindquist, S. (1995). Role of the protein chaperone YDJ1 in establishing Hsp90-mediated signal transduction pathways. *Science* *268*, 1362–1365.
- Kimura, Y., Rutherford, S.L., Miyata, Y., Yahara, I., Freeman, B.C., Yue, L., Morimoto, R.I., and Lindquist, S. (1997). Cdc37 is a molecular chaperone with specific functions in signal transduction. *Genes Dev.* *11*, 1775–1785.
- Kirschke, E., Goswami, D., Southworth, D., Griffin, P.R., and Agard, D.A. (2014). Glucocorticoid receptor function regulated by coordinated action of the Hsp90 and Hsp70 chaperone cycles. *Cell* *157*, 1685–1697.
- Kitagawa, K., Skowrya, D., Elledge, S.J., Harper, J.W., and Hieter, P. (1999). SGT1 encodes an essential component of the yeast kinetochore assembly pathway and a novel subunit of the SCF ubiquitin ligase complex. *Mol. Cell* *4*, 21–33.

- Kornbluth, S., Jove, R., and Hanafusa, H. (1987). Characterization of avian and viral p60src proteins expressed in yeast. *Proc. Natl. Acad. Sci. USA* **84**, 4455–4459.
- Koulov, A.V., LaPointe, P., Lu, B., Razvi, A., Coppinger, J., Dong, M.Q., Matteson, J., Laister, R., Arrowsmith, C., Yates, J.R., 3rd, and Balch, W.E. (2010). Biological and structural basis for Aha1 regulation of Hsp90 ATPase activity in maintaining proteostasis in the human disease cystic fibrosis. *Mol. Biol. Cell* **21**, 871–884.
- Kravats, A.N., Hoskins, J.R., Reidy, M., Johnson, J.L., Doyle, S.M., Genest, O., Masison, D.C., and Wickner, S. (2018). Functional and physical interaction between yeast Hsp90 and Hsp70. *Proc. Natl. Acad. Sci. USA* **115**, E2210–E2219.
- Kurtz, S., Rossi, J., Petko, L., and Lindquist, S. (1986). An ancient developmental induction: heat-shock proteins induced in sporulation and oogenesis. *Science* **237**, 1154–1157.
- Kushnirov, V.V. (2000). Rapid and reliable protein extraction from yeast. *Yeast* **16**, 857–860.
- Kuzmin, E., VanderSluis, B., Wang, W., Tan, G., Deshpande, R., Chen, Y., Usaj, M., Balint, A., Mattiazzi Usaj, M., van Leeuwen, J., et al. (2018). Systematic analysis of complex genetic interactions. *Science* **360**, 360.
- Lee, P., Rao, J., Fliss, A., Yang, E., Garrett, S., and Caplan, A.J. (2002). The Cdc37 protein kinase-binding domain is sufficient for protein kinase activity and cell viability. *J. Cell Biol.* **159**, 1051–1059.
- Lee, C.T., Graf, C., Mayer, F.J., Richter, S.M., and Mayer, M.P. (2012). Dynamics of the regulation of Hsp90 by the co-chaperone Sti1. *EMBO J.* **31**, 1518–1528.
- Li, J., Richter, K., and Buchner, J. (2011). Mixed Hsp90-cochaperone complexes are important for the progression of the reaction cycle. *Nat. Struct. Mol. Biol.* **18**, 61–66.
- Li, J., Soroka, J., and Buchner, J. (2012). The Hsp90 chaperone machinery: conformational dynamics and regulation by co-chaperones. *Biochim. Biophys. Acta* **1823**, 624–635.
- Liu, Y., Mi, Y., Mueller, T., Kreibich, S., Williams, E.G., Van Drogen, A., Borel, C., Frank, M., Germain, P.L., Bludau, I., et al. (2019). Multi-omic measurements of heterogeneity in HeLa cells across laboratories. *Nat. Biotechnol.* **37**, 314–322.
- Lorenz, O.R., Freiburger, L., Rutz, D.A., Krause, M., Zierer, B.K., Alvira, S., Cuéllar, J., Valpuesta, J.M., Madl, T., Sattler, M., and Buchner, J. (2014). Modulation of the Hsp90 chaperone cycle by a stringent client protein. *Mol. Cell* **53**, 941–953.
- Louvion, J.F., Abbas-Terki, T., and Picard, D. (1998). Hsp90 is required for pheromone signaling in yeast. *Mol. Biol. Cell* **9**, 3071–3083.
- Mani, R., St Onge, R.P., Hartman, J.L., 4th, Giaever, G., and Roth, F.P. (2008). Defining genetic interaction. *Proc. Natl. Acad. Sci. USA* **105**, 3461–3466.
- Mayr, C., Richter, K., Lilie, H., and Buchner, J. (2000). Cpr6 and Cpr7, two closely related Hsp90-associated immunophilins from *Saccharomyces cerevisiae*, differ in their functional properties. *J. Biol. Chem.* **275**, 34140–34146.
- McClellan, A.J., Xia, Y., Deutschbauer, A.M., Davis, R.W., Gerstein, M., and Frydman, J. (2007). Diverse cellular functions of the Hsp90 molecular chaperone uncovered using systems approaches. *Cell* **131**, 121–135.
- McLaughlin, S.H., Sobott, F., Yao, Z.P., Zhang, W., Nielsen, P.R., Grossmann, J.G., Laue, E.D., Robinson, C.V., and Jackson, S.E. (2006). The co-chaperone p23 arrests the Hsp90 ATPase cycle to trap client proteins. *J. Mol. Biol.* **356**, 746–758.
- Meyer, P., Prodromou, C., Hu, B., Vaughan, C., Roe, S.M., Panaretou, B., Piper, P.W., and Pearl, L.H. (2003). Structural and functional analysis of the middle segment of hsp90: implications for ATP hydrolysis and client protein and cochaperone interactions. *Mol. Cell* **11**, 647–658.
- Meyer, P., Prodromou, C., Liao, C., Hu, B., Roe, S.M., Vaughan, C.K., Vlasic, I., Panaretou, B., Piper, P.W., and Pearl, L.H. (2004). Structural basis for recruitment of the ATPase activator Aha1 to the Hsp90 chaperone machinery. *EMBO J.* **23**, 1402–1410.
- Montalibet, J., and Kennedy, B.P. (2004). Using yeast to screen for inhibitors of protein tyrosine phosphatase 1B. *Biochem. Pharmacol.* **68**, 1807–1814.
- Moran Luengo, T., Kityk, R., Mayer, M.P., and Rudiger, S.G.D. (2018). Hsp90 breaks the deadlock of the Hsp70 chaperone system. *Mol. Cell* **70**, 545–552.e549.
- Nathan, D.F., and Lindquist, S. (1995). Mutational analysis of Hsp90 function: interactions with a steroid receptor and a protein kinase. *Mol. Cell. Biol.* **15**, 3917–3925.
- Nathan, D.F., Vos, M.H., and Lindquist, S. (1997). In vivo functions of the *Saccharomyces cerevisiae* Hsp90 chaperone. *Proc. Natl. Acad. Sci. USA* **94**, 12949–12956.
- Nathan, D.F., Vos, M.H., and Lindquist, S. (1999). Identification of SSF1, CNS1, and HCH1 as multicopy suppressors of a *Saccharomyces cerevisiae* Hsp90 loss-of-function mutation. *Proc. Natl. Acad. Sci. USA* **96**, 1409–1414.
- Panaretou, B., Siligardi, G., Meyer, P., Maloney, A., Sullivan, J.K., Singh, S., Millson, S.H., Clarke, P.A., Naaby-Hansen, S., Stein, R., et al. (2002). Activation of the ATPase activity of hsp90 by the stress-regulated cochaperone aha1. *Mol. Cell* **10**, 1307–1318.
- Pearl, L.H., and Prodromou, C. (2006). Structure and mechanism of the Hsp90 molecular chaperone machinery. *Annu. Rev. Biochem.* **75**, 271–294.
- Picard, D., Khursheed, B., Garabedian, M.J., Fortin, M.G., Lindquist, S., and Yamamoto, K.R. (1990). Reduced levels of hsp90 compromise steroid receptor action in vivo. *Nature* **348**, 166–168.
- Prodromou, C., Siligardi, G., O'Brien, R., Woolfson, D.N., Regan, L., Panaretou, B., Ladbury, J.E., Piper, P.W., and Pearl, L.H. (1999). Regulation of Hsp90 ATPase activity by tetratricopeptide repeat (TPR)-domain co-chaperones. *EMBO J.* **18**, 754–762.
- Prodromou, C., Panaretou, B., Chohan, S., Siligardi, G., O'Brien, R., Ladbury, J.E., Roe, S.M., Piper, P.W., and Pearl, L.H. (2000). The ATPase cycle of Hsp90 drives a molecular 'clamp' via transient dimerization of the N-terminal domains. *EMBO J.* **19**, 4383–4392.
- Radli, M., and Rudiger, S.G.D. (2018). Dancing with the diva: Hsp90-client interactions. *J. Mol. Biol.* **430**, 3029–3040.
- Retzlaff, M., Hagn, F., Mitschke, L., Hessling, M., Gugel, F., Kessler, H., Richter, K., and Buchner, J. (2010). Asymmetric activation of the hsp90 dimer by its cochaperone aha1. *Mol. Cell* **37**, 344–354.
- Richter, K., Muschler, P., Hainzl, O., Reinstein, J., and Buchner, J. (2003). Sti1 is a non-competitive inhibitor of the Hsp90 ATPase. Binding prevents the N-terminal dimerization reaction during the atpase cycle. *J. Biol. Chem.* **278**, 10328–10333.
- Richter, K., Walter, S., and Buchner, J. (2004). The Co-chaperone Sba1 connects the ATPase reaction of Hsp90 to the progression of the chaperone cycle. *J. Mol. Biol.* **342**, 1403–1413.
- Riggs, D.L., Roberts, P.J., Chirillo, S.C., Cheung-Flynn, J., Prapapanich, V., Ratajczak, T., Gaber, R., Picard, D., and Smith, D.F. (2003). The Hsp90-binding peptidylprolyl isomerase FKBP52 potentiates glucocorticoid signaling in vivo. *EMBO J.* **22**, 1158–1167.
- Rizzolo, K., Huen, J., Kumar, A., Phanse, S., Vlasblom, J., Kakihara, Y., Zeineddine, H.A., Minic, Z., Snider, J., Wang, W., et al. (2017). Features of the chaperone cellular network revealed through systematic interaction mapping. *Cell Rep.* **20**, 2735–2748.
- Rizzolo, K., Kumar, A., Kakihara, Y., Phanse, S., Minic, Z., Snider, J., Stagljar, I., Zilles, S., Babu, M., and Houry, W.A. (2018). Systems analysis of the genetic interaction network of yeast molecular chaperones. *Mol. Omics* **14**, 82–94.
- Rodina, A., Wang, T., Yan, P., Gomes, E.D., Dunphy, M.P., Pillarsetty, N., Koren, J., Gerecitano, J.F., Taldone, T., Zong, H., et al. (2016). The epichaperome is an integrated chaperone network that facilitates tumour survival. *Nature* **538**, 397–401.
- Roe, S.M., Ali, M.M., Meyer, P., Vaughan, C.K., Panaretou, B., Piper, P.W., Prodromou, C., and Pearl, L.H. (2004). The Mechanism of Hsp90 regulation by the protein kinase-specific cochaperone p50(ccd37). *Cell* **116**, 87–98.
- Röhl, A., Wengler, D., Madl, T., Lagleder, S., Tippel, F., Herrmann, M., Hendrix, J., Richter, K., Hack, G., Schmid, A.B., et al. (2015). Hsp90 regulates the dynamics of its cochaperone Sti1 and the transfer of Hsp70 between modules. *Nat. Commun.* **6**, 6655.

- Sahasrabudhe, P., Rohrberg, J., Biebl, M.M., Rutz, D.A., and Buchner, J. (2017). The plasticity of the Hsp90 co-chaperone system. *Mol. Cell* 67, 947–961.e945.
- Scheuffler, C., Brinker, A., Bourenkov, G., Pegoraro, S., Moroder, L., Bartunik, H., Hartl, F.U., and Moarefi, I. (2000). Structure of TPR domain-peptide complexes: critical elements in the assembly of the Hsp70-Hsp90 multichaperone machine. *Cell* 101, 199–210.
- Schmid, A.B., Lagleder, S., Gräwert, M.A., Röhl, A., Hagn, F., Wandinger, S.K., Cox, M.B., Demmer, O., Richter, K., Groll, M., et al. (2012). The architecture of functional modules in the Hsp90 co-chaperone Sti1/Hop. *EMBO J.* 31, 1506–1517.
- Schneider, C.A., Rasband, W.S., and Eliceiri, K.W. (2012). NIH Image to ImageJ: 25 years of image analysis. *Nat. Methods* 9, 671–675.
- Schopf, F.H., Biebl, M.M., and Buchner, J. (2017). The HSP90 chaperone machinery. *Nat. Rev. Mol. Cell Biol.* 18, 345–360.
- Schopf, F.H., Huber, E.M., Dodt, C., Lopez, A., Biebl, M.M., Rutz, D.A., Muhlhofer, M., Richter, G., Madl, T., Sattler, M., et al. (2019). The co-chaperone Cns1 and the recruiter protein Hgh1 link Hsp90 to translation elongation via chaperoning elongation factor 2. *Mol. Cell* 74, 73–87.e78.
- Schuck, P. (2000). Size-distribution analysis of macromolecules by sedimentation velocity ultracentrifugation and lamm equation modeling. *Biophys. J.* 78, 1606–1619.
- Schuldiner, M., Collins, S.R., Thompson, N.J., Denic, V., Bhamidipati, A., Punna, T., Ihmels, J., Andrews, B., Boone, C., Greenblatt, J.F., et al. (2005). Exploration of the function and organization of the yeast early secretory pathway through an epistatic miniarray profile. *Cell* 123, 507–519.
- Shannon, P., Markiel, A., Ozier, O., Baliga, N.S., Wang, J.T., Ramage, D., Amin, N., Schwikowski, B., and Ideker, T. (2003). Cytoscape: a software environment for integrated models of biomolecular interaction networks. *Genome Res.* 13, 2498–2504.
- Shiau, A.K., Harris, S.F., Southworth, D.R., and Agard, D.A. (2006). Structural analysis of *E. coli* hsp90 reveals dramatic nucleotide-dependent conformational rearrangements. *Cell* 127, 329–340.
- Siligardi, G., Panaretou, B., Meyer, P., Singh, S., Woolfson, D.N., Piper, P.W., Pearl, L.H., and Prodromou, C. (2002). Regulation of Hsp90 ATPase activity by the co-chaperone Cdc37p/p50cdc37. *J. Biol. Chem.* 277, 20151–20159.
- Siligardi, G., Hu, B., Panaretou, B., Piper, P.W., Pearl, L.H., and Prodromou, C. (2004). Co-chaperone regulation of conformational switching in the Hsp90 ATPase cycle. *J. Biol. Chem.* 279, 51989–51998.
- Smith, D.F., and Toft, D.O. (1993). Steroid receptors and their associated proteins. *Mol. Endocrinol.* 7, 4–11.
- Storer, C.L., Dickey, C.A., Galigniana, M.D., Rein, T., and Cox, M.B. (2011). FKBP51 and FKBP52 in signaling and disease. *Trends Endocrinol. Metab.* 22, 481–490.
- Suren, T., Rutz, D., Mößner, P., Merkel, U., Buchner, J., and Rief, M. (2018). Single-molecule force spectroscopy reveals folding steps associated with hormone binding and activation of the glucocorticoid receptor. *Proc. Natl. Acad. Sci. USA* 115, 11688–11693.
- Taipale, M., Krykbaeva, I., Koeva, M., Kayatekin, C., Westover, K.D., Karras, G.I., and Lindquist, S. (2012). Quantitative analysis of HSP90-client interactions reveals principles of substrate recognition. *Cell* 150, 987–1001.
- Tenge, V.R., Zuehlke, A.D., Shrestha, N., and Johnson, J.L. (2015). The Hsp90 cochaperones Cpr6, Cpr7, and Cns1 interact with the intact ribosome. *Eukaryot. Cell* 14, 55–63.
- Tong, A.H., and Boone, C. (2006). Synthetic genetic array analysis in *Saccharomyces cerevisiae*. *Methods Mol. Biol.* 313, 171–192.
- Tong, A.H., Evangelista, M., Parsons, A.B., Xu, H., Bader, G.D., Pagé, N., Robinson, M., Raghibizadeh, S., Hogue, C.W., Bussey, H., et al. (2001). Systematic genetic analysis with ordered arrays of yeast deletion mutants. *Science* 294, 2364–2368.
- Verba, K.A., Wang, R.Y., Arakawa, A., Liu, Y., Shirouzu, M., Yokoyama, S., and Agard, D.A. (2016). Atomic structure of Hsp90-Cdc37-Cdk4 reveals that Hsp90 traps and stabilizes an unfolded kinase. *Science* 352, 1542–1547.
- Wandinger, S.K., Suhre, M.H., Wegele, H., and Buchner, J. (2006). The phosphatase Ppt1 is a dedicated regulator of the molecular chaperone Hsp90. *EMBO J.* 25, 367–376.
- Wang, X., Venable, J., LaPointe, P., Hutt, D.M., Koulov, A.V., Coppinger, J., Gurkan, C., Kellner, W., Matteson, J., Plutner, H., et al. (2006). Hsp90 co-chaperone Aha1 downregulation rescues misfolding of CFTR in cystic fibrosis. *Cell* 127, 803–815.
- Woodford, M.R., Dunn, D.M., Blanden, A.R., Capriotti, D., Loisel, D., Prodromou, C., Panaretou, B., Hughes, P.F., Smith, A., Ackerman, W., et al. (2016). The FNIP co-chaperones decelerate the Hsp90 chaperone cycle and enhance drug binding. *Nat. Commun.* 7, 12037.
- Woodford, M.R., Sager, R.A., Marris, E., Dunn, D.M., Blanden, A.R., Murphy, R.L., Rensing, N., Shapiro, O., Panaretou, B., Prodromou, C., et al. (2017). Tumor suppressor Tsc1 is a new Hsp90 co-chaperone that facilitates folding of kinase and non-kinase clients. *EMBO J.* 36, 3650–3665.
- Xu, Y., and Lindquist, S. (1993). Heat-shock protein hsp90 governs the activity of pp60v-src kinase. *Proc. Natl. Acad. Sci. USA* 90, 7074–7078.
- Zhao, R., Davey, M., Hsu, Y.C., Kaplanek, P., Tong, A., Parsons, A.B., Krogan, N., Cagney, G., Mai, D., Greenblatt, J., et al. (2005). Navigating the chaperone network: an integrative map of physical and genetic interactions mediated by the hsp90 chaperone. *Cell* 120, 715–727.
- Zuehlke, A.D., Reidy, M., Lin, C., LaPointe, P., Alsomairy, S., Lee, D.J., Rivera-Marquez, G.M., Beebe, K., Prince, T., Lee, S., et al. (2017). An Hsp90 co-chaperone protein in yeast is functionally replaced by site-specific posttranslational modification in humans. *Nat. Commun.* 8, 15328.

STAR★METHODS

KEY RESOURCES TABLE

REAGENT or RESOURCE	SOURCE	IDENTIFIER
Antibodies		
eEF2 antibody	Kerafast	Cat# ED7002
HA antibody	Sigma-Aldrich	Cat# H3663; RRID: AB_262051
Hsp26 antibody	Pineda	N/A
Hsp82/Hsc82 antibody	Pineda	N/A
PGK1 antibody	Invitrogen	Cat# 459250; RRID: AB_2532235
pTyr antibody	Antikörper-online.de	Cat# ABIN94452; RRID: AB_10767083
Anti-rabbit antibody	Sigma-Aldrich	Cat# A0545; RRID: AB_257896
Anti-mouse antibody	Sigma-Aldrich	Cat# A4789; RRID: AB_258201
Chemicals, Peptides, and Recombinant Proteins		
11-deoxycorticosterone	Sigma-Aldrich	Cat# D6875
Aldosterone	Sigma-Aldrich	Cat# A9477
ATTO488-maleimide	ATTO-TEC	Cat# AD 488-45
L-Canavanine sulfate	Sigma-Aldrich	Cat# C9758
Cycloheximide	Sigma-Aldrich	Cat# C4859
Dexamethasone	Sigma-Aldrich	Cat# D4902
Doxycyclin	Sigma-Aldrich	Cat# D1822
Hygromycin B	Sigma-Aldrich	Cat# 10843555001 Roche
Nourseothricin sulfate	Jena Biosciences	Cat# AB-102XL
ortho-Nitrophenyl- β -galactoside (ONPG)	Sigma-Aldrich	Cat# N1127
Radicalol	Sigma-Aldrich	Cat# R2146
Puromycin dihydrochloride	Sigma-Aldrich	Cat# P8833
S ³⁵ -Methionine	Hartman Analytic	Cat# KSM-01
L-4-Thialysine hydrochloride	Sigma-Aldrich	Cat# A2636
ATP γ S	Sigma-Aldrich	Cat# A1388
Experimental Models: Organisms/Strains		
WT Yeast BY4741; MATa; ura3 Δ 0; leu2 Δ 0; his3 Δ 1; met15 Δ 0	Euroscarf	Cat# Y00000
Y8205 MAT α can1 Δ ::STE2pr-Sp_his5; lyp1 Δ ::STE3pr-LEU2; his3 Δ 1; leu2 Δ 0; ura3 Δ 0	C. Boone	N/A
sti1 Δ BY4741; MATa; ura3 Δ 0; leu2 Δ 0; his3 Δ 1; met15 Δ 0; YOR027w::KanMX4	Euroscarf	Cat# Y01803
cdc37-DAmP BY4741; MATa; ura3 Δ 0; leu2 Δ 0; his3 Δ 1; met15 Δ 0; cdc37-DAmP::KanMX4	Dharmacon	Cat# YSC5093-213595844
cns1-DAmP BY4741; MATa; ura3 Δ 0; leu2 Δ 0; his3 Δ 1; met15 Δ 0; cns1-DAmP::KanMX4	Dharmacon	Cat# YSC5093-21359678
tah1 Δ BY4741; MATa; ura3 Δ 0; leu2 Δ 0; his3 Δ 1; met15 Δ 0; YCR060w::KanMX4	Euroscarf	Cat# Y07189
pih1 Δ BY4741; MATa; ura3 Δ 0; leu2 Δ 0; his3 Δ 1; met15 Δ 0; YHR034c::KanMX4	Euroscarf	Cat# Y00997
cpr6 Δ BY4741; MATa; ura3 Δ 0; leu2 Δ 0; his3 Δ 1; met15 Δ 0; YLR216c::KanMX4	Euroscarf	Cat# Y04165
cpr7 Δ BY4741; MATa; ura3 Δ 0; leu2 Δ 0; his3 Δ 1; met15 Δ 0; YJR032w::KanMX4	Euroscarf	Cat# Y06830

(Continued on next page)

REAGENT or RESOURCE	SOURCE	IDENTIFIER
sba1Δ BY4741; MATa; ura3Δ0; leu2Δ0; his3Δ1; met15Δ0; YKL117w::KanMX4	Euroscarf	Cat# Y04967
aha1Δ BY4741; MATa; ura3Δ0; leu2Δ0; his3Δ1; met15Δ0; YDR214w::KanMX4	Euroscarf	Cat# Y03573
hch1Δ BY4741; MATa; ura3Δ0; leu2Δ0; his3Δ1; met15Δ0; YNL281w::KanMX4	Euroscarf	Cat# Y01163
ppt1Δ BY4741; MATa; ura3Δ0; leu2Δ0; his3Δ1; met15Δ0; YGR123c::KanMX4	Euroscarf	Cat# Y04753
WT BY4741xY8205; MATa; ura3Δ0; leu2Δ0; can1Δ::STE2pr-Sp_his5; his3Δ1	This work	N/A
yfg1Δ/yfg2Δ; MATa; can1Δ::STE2pr-Sp_his5; his3Δ1; leu2Δ0; ura3Δ0; yfg1Δ::NatMX; yfg2Δ::KanMX4	This work	N/A
yfg2Δ/yfg1Δ; MATa; can1Δ::STE2pr-Sp_his5; his3Δ1; leu2Δ0; ura3Δ0; yfg2Δ::NatMX; yfg1Δ::KanMX4	This work	N/A
yfg1*/yfg2Δ; MATa; can1Δ::STE2pr-Sp_his5; his3Δ1; leu2Δ0; ura3Δ0; YFG1::DAmP-NatMX; yfg2Δ::KanMX4	This work	N/A
yfg2*/yfg1Δ; MATa; can1Δ::STE2pr-Sp_his5; his3Δ1; leu2Δ0; ura3Δ0; YFG2::DAmP-NatMX; yfg1Δ::KanMX4	This work	N/A
yfg1*/yfg2*; MATa; can1Δ::STE2pr-Sp_his5; his3Δ1; leu2Δ0; ura3Δ0; YFG1::DAmP-NatMX; YFG2::DAmP-KanMX4	This work	N/A
yfg2*/yfg1*; MATa; can1Δ::STE2pr-Sp_his5; his3Δ1; leu2Δ0; ura3Δ0; YFG2::DAmP-NatMX; YFG1::DAmP-KanMX4	This work	N/A
<i>All possible combinations with yfg1 and yfg2 as sti1, cdc37, cns1, tah1, pih1, cpr6, cpr7, sba, aha1, hch1 or ppt1</i>	This work	N/A
R1158; URA3::CMV-tTA; MATa; his3Δ1; leu2Δ0; met15Δ0	Open Biosystems	N/A
cpr7Δ R1158; URA3::CMV-tTA; MATa; his3Δ1; leu2Δ0; met15Δ0; cpr7::NatNT2	(Schopf et al., 2019)	N/A
tet07-CNS1 R1158; URA3::CMV-tTA; MATa; his3Δ1; leu2Δ0; met15Δ0; pCNS1::kanR-tet07-TATA	Dharmacon	Cat# TH3647
tet07-CNS1 cpr7Δ R1158; URA3::CMV-tTA; MATa; his3Δ1; leu2Δ0; met15Δ0; pCNS1::kanR-tet07-TATA; cpr7::NatNT2	(Schopf et al., 2019)	N/A
tet07-CNS1 sti1Δ; URA3::CMV-tTA; MATa; his3Δ1; leu2Δ0; can1Δ::STE2pr-Sp_his5; pCNS1::NatMX-tet07-TATA; sti1::hphNT1	C. Dodt	N/A
tet07-CNS1 sti1Δ cpr7Δ; URA3::CMV-tTA; MATa; his3Δ1; leu2Δ0; can1Δ::STE2pr-Sp_his5; pCNS1::NatMX-tet07-TATA; cpr7::hphNT1; sti1::KanMX4	C. Dodt	N/A
Recombinant DNA		
p415-GPD GR	This work	N/A
p415-GPD MR	This work	N/A
p413-GPD GR	(Sahasrabudhe et al., 2017)	N/A

(Continued on next page)

Continued

REAGENT or RESOURCE	SOURCE	IDENTIFIER
p413-GPD HA-GR	(Sahasrabudhe et al., 2017)	N/A
p413-GPD HA-MR	(Sahasrabudhe et al., 2017)	N/A
pUCΔSS-26X	J.F. Louvion	N/A
p416-GAL1 v-Src	This work	N/A
p416-GALS v-Src	This work	N/A
p416-GAL1 HA-v-Src	This work	N/A
p415-GPD Aha1	This work	N/A
p415-GPD Hch1	This work	N/A
p415-GPD Aha1-D53K	This work	N/A
p415-GPD Hch1-D53K	This work	N/A
p415-GPD Cdc37	This work	N/A
p415-GPD Sti1	This work	N/A
p415-GPD Sti1-N39A/N435A	This work	N/A
pYes-ΔN-Ste11	(Louvion et al., 1998)	N/A
Software and Algorithms		
Astra 5.3.4.20	Wyatt Technology	N/A
Cytoscape 3.6.1	(Shannon et al., 2003)	N/A
ImageJ 1.50i	(Schneider et al., 2012)	N/A
OriginPro 2016G	OriginLab	N/A
SedFit 14.1	(Schuck, 2000)	N/A
Sedview 1.1	(Hayes and Stafford, 2010)	N/A

RESOURCE AVAILABILITY

Lead Contact

Further information and requests for resources and reagents should be directed to and will be fulfilled by the lead contact, Prof. Dr. Johannes Buchner (johannes.buchner@tum.de).

Materials Availability

Plasmids and yeast strains generated in this work are available from the lead contact upon reasonable request.

Data and Code Availability

This study did not generate/analyze unique code or datasets.

EXPERIMENTAL MODEL AND SUBJECT DETAILS

In this study, yeast strains derived from BY4741, Y8205 and R1158 were used. Single mutants were obtained from Euroscarf or Dharmacon. KOs or KDs were generated by linear knockout or mating following synthetic genetic array (SGA) screening procedures (Tong and Boone, 2006; Tong et al., 2001) and are briefly outlined here. Yeast was cultured in YPD medium or selective dropout medium at 30°C unless specified otherwise.

METHOD DETAILS

Yeast Transformation

High-efficiency transformation into yeast was done following a previously published protocol (Gietz and Schiestl, 2007). A yeast culture was grown in 50 mL YPD medium from a starting OD₆₀₀ from 0.15 for 4.5 h at 30°C while shaking. Cells were harvested at 3000 x g for 5 min at room temperature, washed with 25 mL water and the resuspended in 1 mL 0.1 M lithium acetate. The cells were harvested and then resuspended in 500 μL of 0.1 M lithium acetate. For each transformation, 50 μL of this sample were harvested, 240 μL PEG-3350, 36 μL of 1 M lithium acetate, 10 μL ssDNA and 72 – X μL H₂O were added with X representing the volume of DNA solution. After mixing, the sample was incubated at 30°C for 30 min and at 42°C for 30 min. Cells were then harvested at 4000 x g for 30 s and plated on selective medium.

Generation of Yeast Strains

Single KO and diploid DAMP (Decreased Abundance by mRNA Perturbation) strains for yeast co-chaperones were obtained from Euroscarf (Oberursel, Germany) or Dharmacon (Lafayette, USA) as derivatives of BY4741 (Schuldiner et al., 2005). Diploid DAMP strains were sporulated and tetrads were picked to obtain haploid MAT α DAMP strains. Throughout the manuscript, the DAMP strains are referred to with asterisks, (e.g., *cns1**). To generate double mutants, first the KanMX4 cassette was swapped to the nourseothricin resistance cassette by transforming yeast cells with the 50 μ L of PCR product of the NatMX cassette (F:ACATGGAGGCC CAGAATACCCT; R: CAGTATAGCGACCAGCATTAC) and selecting for nourseothricin resistance (Janke et al., 2004). The resulting strains were mated with the strain Y8205 (Charles Boone Lab, University of Toronto) and then sporulated on sporulation medium (Tong and Boone, 2006) for 5 days at 20°C. Haploid MAT α spores were selected by incubation on medium containing L-canavanine (50 μ g/mL), L-4-thialysine (50 μ g/mL) and lacking arginine, leucine, and lysine according to the SGA selection procedure (Tong and Boone, 2006; Tong et al., 2001). To generate double mutant strains, the resulting MAT α strains were mated with the original KO/KD strains, diploids were sporulated as described and haploid MAT α strains were selected on selective medium containing L-canavanine (50 μ g/mL) and L-4-thialysine (50 μ g/mL), but lacking histidine, arginine, and lysine (Tong and Boone, 2006). Single and double mutants were then selected by incubation on $-His/Arg/Lys +L-canavanine/L-4-thialysine$ medium supplemented with 100 μ g/mL nourseothricin and/or 200 μ g/mL gentamicin. KO or KD of the target co-chaperones was confirmed by Western-Blot and/or colony PCR.

The *tet07-CNS1* strain was obtained from the yeast Tet-promoters Hughes Collection (Dharmacon, Lafayette, USA) in the R1158 background. To generate a *tet07-CNS1/cpr7 Δ /sti1 Δ* triple mutant, the mating type of *tet07-CNS1* was switched by mating with the Y8205 strain and the KanMX4 cassette was swapped to a NatMX cassette. The *cpr7 Δ* mutation was introduced by inserting the *hphNT1* resistance cassette using the Knop toolbox (Janke et al., 2004). This strain was then mated with the Euroscarf BY4741 *sti1 Δ* strain and the haploid triple mutant was selected as described above (Tong and Boone, 2006; Tong et al., 2001).

SEM

SEM was performed based on a protocol published elsewhere (Spector et al., 1998). Stationary phase yeast cells were harvested at 4000 x g for 5 min and washed once with 500 μ L of PBS. Subsequently, the cells were resuspended in 2.5% glutaraldehyde in PBS and incubated at room temperature for 1 h while shaking. Subsequently, the cells were pelleted again and washed with PBS. Then, the cells were resuspended in 300 μ L PBS and 30 μ L were spotted on a Thermanox Plastic Coverslip (ThermoFisher Scientific). After incubation at room temperature for 2 min, the slides were washed in a Petri dish with 7.5 mL 50% ethanol, followed by washing steps with 7.5 mL 70% ethanol, 7.5 mL 80% ethanol, 7.5 mL 95% ethanol and thrice with 7.5 mL 100% ethanol. The slides were dried in a vacuum chamber over-night. Before microscopy, the cells were sputtered with gold and SEM was performed with a JEOL 5900 LV microscope (JEOL, Eching, Germany). Pictures of the cells were taken at a constant voltage of 20 kV at $2-3 \times 10^{-6}$ Torr vacuum.

SHR Activity Screening

GR and MR activity in yeast was determined in a 96-well format as previously described (Sahasrabudhe et al., 2017). Briefly, yeasts transformed with the SHR expression plasmid and the β -galactosidase reporter plasmid were grown over-night at 30°C while shaking at 150 rpm. Cells were then diluted 1:10 in media containing 10 μ M DOC (11-deoxycorticosterone) or 10 μ M aldosterone for GR or MR, respectively, and grown to stationary phase over-night at 30°C while shaking at 150 rpm. Then, 50 μ L of the cell suspension were transferred to a clear-bottom 96-well plate and harvested at 3000 x g. The supernatant was discarded and the cells were permeabilized in 150 μ L of resuspension buffer (Na₂HPO₄ 82 mM, NaH₂PO₄ 12 mM, 0.1% SDS, pH 7.5) while shaking at 900 rpm for 15 min at room temperature. The enzymatic reaction was induced by addition of ONPG (ortho-nitrophenyl- β -galactoside, Sigma-Aldrich) to a final concentration of 1 mg/mL and the increase of the absorption at 420 nm was monitored for 30-40 min in a Tecan sunrise plate reader. The slope of the linear region was determined using Origin Pro 2016G. All measurements were performed in at least four and usually eight biological replicates as indicated in the respective figure legends.

Viability Screening

For viability screening, cells were grown to stationary phase over-night. 5 OD₆₀₀ units were then harvested at 4000 x g, washed with 1 mL of water and resuspended to a final concentration of 10 OD₆₀₀/mL. Dilution series with 10-fold serial dilutions starting from 1 OD₆₀₀/mL were produced and then spotted on YPD plates. Every agar plate contained the WT and the single mutant as control and only strains that were grown on the same plate were compared. Viability was determined after 48 h and 72 h of incubation at 30°C. To obtain an objective measure in addition to the visual analysis, we quantified spot-density of a suitable dilution using the ImageJ software and normalized the density to the wild-type, spotted on the same plate.

v-Src Activity Screening

Yeast strains harboring v-*Src* under the GAL1 or the weaker GAL-S promoter were grown in selective media over-night. 5 OD₆₀₀ units were then prepared as described above. Dilution series with 5-fold or 10-fold serial dilutions starting from 1 OD₆₀₀/mL were produced and then spotted on selective agar containing either 2% D-glucose (D-Glc) or 2% D-galactose (D-Gal). Each plate contained the wild-type and the single mutant strain as control and only strains that were grown on the same plate were compared. Cell growth was documented after 48 h and 72 h. To provide an objective quantification in addition to the visual analysis, colony density of the spots

in appropriate dilutions was calculated using ImageJ and the spot density on the D-Gal containing plate was normalized to the uninduced control on glucose-containing plates. Screening was performed with the GAL1 promoter once and additionally with the GAL-S promoter in duplicates or triplicates.

Ste11 Activity Analysis

The activity of Ste11 kinase in yeast was analyzed using a previously described constitutively active Ste11 mutant (Δ N-Ste11) (Louvion et al., 1998). Cells were grown to stationary phase over-night and then spotted in 10-fold serial dilutions as described above on selective agar containing 2% D-galactose as the only carbon source or 2% D-glucose as control.

Phosphotyrosine Kinase Activity Measurements

Tyrosine kinase activity of v-Src was quantified as previously described (Sahasrabudhe et al., 2017). Briefly, cells were grown to stationary phase in minimal medium with 2% raffinose as the only carbon source for about 24 h. Then, the culture was diluted to an OD₆₀₀ of about 0.1 and grown overnight. In the morning a culture was inoculated to an OD₆₀₀ of 0.3 and cells were grown for 5–8 h to reach an OD₆₀₀ of 0.8 before induction of v-Src expression with 2% D-galactose (D-Gal). v-Src expression was allowed to occur for 4 h. Samples of 1–2 OD₆₀₀ units were then harvested by trichloroacetic acid (TCA) precipitation (Baerends et al., 2000). Briefly, TCA was added to a final concentration of 20% and samples were frozen at -80°C for at least 30 min. After thawing, cells were pelleted, washed twice with -20°C cold 80% acetone and then dried at 30°C . The dried cells were then lysed by addition of 1% SDS in 0.1 M NaOH, Laemmli buffer was added and cells were boiled at 95°C for 5 min prior to SDS-PAGE and Western Blot.

Aggregate Isolation

To isolate whole-proteome or eEF2 pellet and supernatant fractions, yeast cultures were grown to early logarithmic phase (OD₆₀₀ of 0.8) for harvesting. For heat-shocked samples, stationary-phase cultures were diluted to an OD₆₀₀ of 0.3 and incubated at 30°C for 1 h before the samples were transferred to 42°C or kept at 30°C for 3 h until an OD₆₀₀ of approximately 0.8–1.2 was reached. For radicicol-treated samples, an over-night culture was diluted to a starting OD₆₀₀ of 0.3, incubated at 30°C for 1 h and then treated either with 20 μM radicicol or DMSO for 3 h until an OD₆₀₀ of 0.8–1.2 was reached. HA-v-Src samples were grown to stationary phase as described for phosphotyrosine quantification. HA-v-Src expression was induced by addition of 2% D-Gal and expression took place for 6 h. If applicable, 5 μM of radicicol or DMSO were added together with D-Gal for induction. 30–40 OD₆₀₀ units were harvested at 3000 \times g for 5 min, washed with PBS and resuspended in lysis buffer (50 mM Tris, 150 mM NaCl, 5 mM MgCl₂, 5% glycerol, pH 8.0) supplemented with 1 \times Protease Inhibitor Mix G (Serva), 1 mM PMSF and 5 mM EDTA. Cells were lysed by glass-bead disruption with 4 on/off cycles consisting of 2 min of shaking in a Retsch mixer mill at 30 Hz and 2 min off time between cycles. The lysate was pre-cleared by centrifugation at 500 \times g for 1 min at 4°C . Protein concentration was normalized using Bradford reagent and 50 μl of the sample volume were centrifuged at 18,000 \times g at 4°C to separate supernatant and pellet. The pellet was then washed twice with lysis buffer before resuspension in resuspension buffer (1% SDS, 6 M urea, 50 mM Tris-HCl, 1 mM EDTA, pH 7.5). The samples were then subjected to SDS-PAGE and Western-Blot following standard procedures.

Cycloheximide Chase

For cycloheximide chase of HA-GR and HA-MR, yeast cultures were grown to logarithmic phase (OD₆₀₀ = 0.8) and then treated with 100 $\mu\text{g}/\text{mL}$ cycloheximide. For cycloheximide chase experiments with HA-v-Src, cells were grown to logarithmic phase following the described protocol, HA-v-Src expression was induced for 4 h and then 100 $\mu\text{g}/\text{mL}$ of cycloheximide were added. In samples that contained radicicol, the inhibitor was added together with cycloheximide at a final concentration of 5 μM . At the indicated time points, 1–5 OD₆₀₀ units were precipitated by addition of TCA as described above and samples were subjected to SDS-PAGE and Western-Blot.

Protein Expression and Purification

Hsp82, Hch1 and Aha1 were purified as previously described (Li et al., 2011; Schmid et al., 2012). The GR-LBDm was purified as published (Lorenz et al., 2014).

Analytical Ultracentrifugation

For sedimentation velocity experiments, the GR-LBDm was randomly labeled with Atto488-maleimide (ATTO-TEC) on cysteines. Experiments were performed in a ProteomLab Beckman XL-A centrifuge (Beckman Coulter, Brea, California) equipped with an AVIV fluorescence detection unit (Aviv Inc., Lakewood, USA) using 500 nM of the labeled component and 3 μM or 6 μM of unlabeled components as indicated in the figure legend. Experiments were conducted in aUC buffer (20 mM HEPES, 20 mM KCl, 5 mM MgCl₂, 5 mM DTT, pH 7.5) supplemented with 2 mM ATP- γ S and 50 μM dexamethasone if the sample contained the GR-LBD. Data analysis was performed using SedView (Hayes and Stafford, 2010), SedFit (Schuck, 2000) and Origin Pro 2016G.

³⁵S-Methionine Incorporation

To quantify the effect of Hsp90 co-chaperones on the rate of protein biosynthesis, ³⁵S-methionine incorporation was monitored based on a published protocol (Esposito and Kinzy, 2014). Briefly, cells were grown to log phase from a starting OD₆₀₀ of 0.2 to

an OD₆₀₀ of 0.8, harvested, washed with PBS and resuspended in pre-warmed selective medium lacking methionine to a final OD₆₀₀ of 1. Cells were supplemented with 10 μCi L-S³⁵-methionine and 60 μM cold L-methionine and grown at 30°C for 90 min. Cells equivalent to 1 OD₆₀₀ were then harvested, washed once with 1 mL H₂O + 100 μg/mL cycloheximide and lysed as described elsewhere (Kushnirov, 2000). The proteins were separated by SDS-PAGE, the gels were dried and the autoradiography was analyzed using a Typhoon 9200 (GE Healthcare) multimode scanner. Densitometry analysis was performed using ImageJ and the values were normalized to the WT control.

Genetic Interactions

Genetic interactions were quantified using the ϵ -Score. For fitness analysis, the ϵ -Score was defined as $\epsilon = f_{ab} - f_a * f_b$, where f_{ab} indicates the fitness of the double mutant and f_a and f_b represent the fitness of the individual mutants (Elena and Lenski, 1997; Mani et al., 2008). To provide a measure of v-Src activity, the ϵ -Score was defined as $\epsilon = f_a * f_b - f_{ab}$, with f_{ab} indicating double mutant fitness and f_a and f_b denoting the fitness of the individual mutants. For receptor activity (for GR and MR) measurements, the ϵ -Score was used as stated in the respective Results section. For normalization, the ϵ -Score was divided by the expected activity $\epsilon\text{-Score}_{\text{norm}} = \epsilon\text{-Score} / (f_a * f_b)$.

QUANTIFICATION AND STATISTICAL ANALYSIS

Statistical parameters are reported in the figures and figure legends. Statistical significance was assigned by using a two-sample t test. p values below 0.05 were classified as significant (n.s.: $p > 0.05$; * $p \leq 0.05$; ** $p \leq 0.01$; *** $p \leq 0.001$).